

SANDIA REPORT

SAND2017-5297
Unlimited Release
Printed May 2017

Shock-Induced Solid-State reactions in Powders: An Experimentally-Based Reassessment

M.B. Boslough, S.A. Silling S.H. Fischer*, D.E. Cox*, and W.B. Vandermolen*

* Retired

Prepared by
Sandia National Laboratories
Albuquerque, New Mexico 87185 and Livermore, California 94550

Sandia National Laboratories is a multimission laboratory managed and operated by National Technology & Engineering Solutions of Sandia, LLC., a wholly owned subsidiary of Honeywell International, Inc., for the U.S. Department of Energy's National Nuclear Security Administration under contract DE-NA0003525.



Sandia National Laboratories

Issued by Sandia National Laboratories, operated for the United States Department of Energy by National Technology and Engineering Solutions of Sandia, LLC.

NOTICE: This report was prepared as an account of work sponsored by an agency of the United States Government. Neither the United States Government, nor any agency thereof, nor any of their employees, nor any of their contractors, subcontractors, or their employees, make any warranty, express or implied, or assume any legal liability or responsibility for the accuracy, completeness, or usefulness of any information, apparatus, product, or process disclosed, or represent that its use would not infringe privately owned rights. Reference herein to any specific commercial product, process, or service by trade name, trademark, manufacturer, or otherwise, does not necessarily constitute or imply its endorsement, recommendation, or favoring by the United States Government, any agency thereof, or any of their contractors or subcontractors. The views and opinions expressed herein do not necessarily state or reflect those of the United States Government, any agency thereof, or any of their contractors.

Printed in the United States of America. This report has been reproduced directly from the best available copy.

Available to DOE and DOE contractors from
U.S. Department of Energy
Office of Scientific and Technical Information
P.O. Box 62
Oak Ridge, TN 37831

Telephone: (865) 576-8401
Facsimile: (865) 576-5728
E-Mail: reports@osti.gov
Online ordering: <http://www.osti.gov/scitech>

Available to the public from
U.S. Department of Commerce
National Technical Information Service
5301 Shawnee Rd
Alexandria, VA 22312

Telephone: (800) 553-6847
Facsimile: (703) 605-6900
E-Mail: orders@ntis.gov
Online order: <http://www.ntis.gov/search>



Shock-Induced Solid-State Reactions in Powders: An Experimentally-Based Reassessment

M.B. Boslough, Org 01446
S.A. Silling, Org 01444
S.H. Fischer*, D.E. Cox*, and W.B. Vandermolen*
Sandia National Laboratories
P. O. Box 5800
Albuquerque, New Mexico 87185-MS1320
*retired

Abstract

We have performed a series of ten planar impact experiments on six different materials, including certain reactive powders and two inert materials, using Sandia's 89-mm powder gun at the STAR facility. Time-resolved particle-velocity histories were determined during each of the experiments from one or more VISAR measurements. We have analyzed the results of these measurements 1) by using jump conditions to determine shock and first reshock states and 2) by comparing measured particle velocity histories to synthetic histories predicted by one-dimensional computational analyses using the CTH shock physics code with various models for inert and reactive materials. These comparisons are consistent with the conclusion for these particular reactive powders, that for the duration of shock loading either 1) there is insignificant reaction or 2) the products of any reaction are indistinguishable from the reactants under the experimental conditions. Shock and reshock states were extracted for shock pressures between 5 and 40 GPa. Densities were at or greater than the theoretical maximum zero-pressure density of the starting mixture. This result would be expected if there were no reaction or negligible reaction for the first two shock states. Two experiments were performed on one reactive powder in a "ring-down" geometry to look for evidence of vapor production on pressure release. In both cases, the measured velocity continued to increase slowly over a period of microseconds for the duration of the experiment. This observation suggests that vapor is produced along the release path, but information about the mechanism for vapor production cannot be extracted from these data. While it is possible that vapor is produced by a shock-induced reaction involving more than one of the original constituents, a simpler interpretation is that the vapor is made up of products of shock-induced decomposition reactions and/or simple vaporization of the constituents as would be expected to take place under the conditions of these experiments. Other sources of vapor could be water adsorbed on grain surfaces and air originally in the voids. Thus it is not necessary to invoke significant recombination reactions to explain the data. However, in the absence of ring-down control experiments, the possibility remains open. These conclusions are different from those of previous workers, but reassessment of a subset of the earlier data yields results consistent with the

present work, i.e., the shock compression data do not provide evidence for strong exothermic reactions.

ACKNOWLEDGMENTS

R.T. Patton and E.J. Mulligan assisted in mixing the sample powders. H.M. Anderson assembled the target fixtures, and the powders were pressed by C.E. Haynes. R.L. Moody assisted with the powder gun experiments and data transfer, and D.A. Crawford provided help in running his new VISAR data reduction program. This report was written in 1995. It was re-formatted with light editing in 2017 by C. Trujillo.

TABLE OF CONTENTS

1.	Introduction.....	9
2.	Experimental.....	11
3.	Computational.....	15
4.	Results and Discussion.....	21
5.	Earlier Experimental Work.....	39
6.	Conclusions.....	45
7.	Recommendations.....	47
REFERENCES		49

FIGURES

Figure 2.1 -	Nominal projectile-target configuration. Details for each experiment are listed in Table 2.1 and Figs. 5.1-5.10.	11
Figure 3.1 -	Pressure-volume curves (top) and a pressure-compression curves (bottom) for four values of A. in the CTH model. The segment <i>OC</i> represents partially crushed reactant.	16
Figure 3.2 -	Reaction kinetics model. Top: pressure history at a point, showing a shock wave. Bottom: reaction rate history at the point.	17
Figure 3.3 -	Determination of maximum extent of reaction.	18
Figure 3.4 -	Reaction time as a function of maximum pressure.	18
Figure 4.1 -	Schematic P-u diagram and experimental configuration for experiment TWP-2 (RS234). Bottom : Measured particle velocity history at point indicated in upper right-hand comer, and CTH prediction of particle velocity history using inert model.	22
Figure 4.2 -	TWP (neoprene) data, displayed as in Fig. 4.1	23
Figure 4.3 -	TWP-3 (Aluminum, powder) data.	24
Figure 4.4 -	TWP-6 (GA134) data.	25
Figure 4.5 -	TWP-9 (C0104) data.	26
Figure 4.6 -	TWP-4 (RS234) data	27
Figure 4.7 -	TWP-7 (RS234) data, with two calculated velocity histories, one with an inert model and one with a reactive model.	28
Figure 4.8 -	TWP-8 (CS691) data. Two independent velocity measurements are shown.	29
Figure 4.9 -	TWP-10 (RS234) data. Two independent free-surface velocity measurements are shown along with inert and reactive calculated velocities.	30
Figure 4.10 -	TWP-11 (RS234) data	31
Figure 4.11 -	Shock and reshock states of five RS234 experiments transformed to P- V plane. The vertical dashed line denotes the fully crushed volume of the reactants at zero pressure.	37
Figure 5.1 -	Schematic representation of experimental configuration of PVDF experiments.	39

Figure 5.2 – Schematic loading history in PVDF experiments, showing distance-time diagram, stress history, and stress/particle velocity-diagram.	40
Figure 5.3 – Data from unpublished PVDF experiments on 50% TMD reactive powders and ballotechnic curve defined by Graham et al. (1993) with P-V states re- calculated from original data.	43

TABLES

Table 2.1: Experimental Parameters.....	13
Table 3.1: Numerical Parameters	19
Table 4.1: Shock and Reshock State Parameters for RS234 Experiments	36

NOMENCLATURE

Abbreviation	Definition
Abbreviation	Definition
P	Pressure
U	Shock Velocity
u	Particle Velocity
ρ	Density
V	Specific volume (reciprocal of density)
λ	Reaction parameter (fraction of reacted material), $0 \leq \lambda \leq 1$
μ	compression, (defined by $\mu = (V/V_0) - 1$)
t	Time
TMD	Theoretical Maximum Density
VISAR	Velocity Interferometer System for Any Reflector
PVDF	Polyvinylidene difluoride
PTFE	Polytetrafluoroethylene (teflon)
LiF	Lithium fluoride
OFHC	Oxygen-free, high-conductivity (copper)
STAR	Shock Technology and Applied Research (Facility)

1. INTRODUCTION

Shock-induced chemical reactions have been the subject of extensive study in certain powder mixtures (e.g. Horie 1986, Graham 1988, Horie and Kipp 1988, Boslough 1990). These experiments have led some workers to the conclusion that strong exothermic solid-state reactions can take place in some of these mixtures (see, for example, Graham 1988). However, in mixtures with the largest heats of reaction, all the equilibrium products are in the liquid or vapor phase (Boslough 1990, 1992a). Unlike many of the synthesis reactions surveyed by Graham et al. (1986), shock-induced reactions in these more energetic mixtures cannot be solid-state reactions. In the conventional sense, the term "solid-state chemistry" refers to reactions for which the products are in the solid state (Schmalzreid 1981). This is because solid-state reactions require local transport of matter in the crystalline phase. Use of the term "shock-induced solid-state chemistry" in reference to reactions yielding liquid or vapor products is a misnomer.

For many of the reactive powders that have been examined, the equilibrium mixture of product phases remains condensed as liquid until the pressure is released (Boslough 1990). Thus the effects of the reaction on any measured kinematic variable associated with the high pressure states (pressure, shock velocity, particle velocity) will be subtle for many reactions. Such measurements will be most sensitive to a reaction in mixtures in which the compressed density of the product phases deviates the most from that of the reactants (Boslough 1992a). In mixtures where there is no volume change associated with the reaction, such measurements will not yield information about the existence or nonexistence of a reaction. If there is a phase change such as vaporization on release, or a significant difference in compressibility, then release states will yield information. Since many of the reactions of interest are highly exothermic, temperature measurements would be the most sensitive. However, these are subject to severe complications when applied to powders with grain sizes exceeding several microns (Boslough 1992b, Yoshida 1994).

Although one of the powder mixtures tested in this series has been tested in previous experiments, little is certain about the existence, sequence, or rate of shock-induced chemical reactions. Some researchers who have studied these types of powder mixtures have interpreted their data to indicate sub-microsecond reaction times. Temperature measurements were used to support this view (Boslough and Graham 1985, Hornig et al. 1986, Boslough 1990), but further analysis demonstrates that the evidence for reaction in coarser-grained ($> 10 \mu\text{m}$ -diameter particles) was based on localized high temperatures that were also present in inert control experiments (Boslough 1992b). More recently, data from PVDF gauges have been used to support the contention that rapid reactions take place in a variety of powder mixtures (Graham et al. 1993, Dunbar et al. 1994). In Section 5 we will discuss the analysis of these experiments in detail and explain why we believe the data do not necessarily support this conclusion.

The new experiments described in this report were performed to critically evaluate the hypothesis that certain materials undergo rapid, highly energetic shock-induced chemical reactions at or immediately after passage of a shock wave. The plan was to evaluate, under a variety of loading conditions, one mixture that had previously been reported to react (RS234), and to survey new mixtures chosen on the basis of their predicted likelihood to react under shock loading. The experiments were designed to be one-dimensional until rarefactions and multidimensional effects interfered after about $3 \mu\text{s}$ of reading time. Control experiments were carried out on two single-

species compositions so that the predictive capability of computational analyses could be determined and possible time dependences in particle-velocity histories unrelated to chemical reactivity could be assessed.

A computational model was developed using a purely mechanical equation of state and an empirical reaction model. The model was used to calculate synthetic particle velocity histories, which could then be compared to the experimentally determined profiles. However, when highly porous powders are shocked to pressures in the 10 GPa range, the resulting pressure has a relatively large thermal component, so a purely mechanical description is not adequate. Thus, comparison of synthetic to measured velocity histories may yield significant differences on this basis alone, which may mask any evidence, or lack of evidence, for reaction products.

Because shock velocities through the powders can be extracted from transit times, we were also able to calculate shock and re-shock states by means of impedance match solutions (Hugoniot analysis). These states were transformed and plotted in the pressure-volume plane. A Hugoniot equation of state can be constructed from these data, which makes it possible to determine whether or not a shock-induced reaction is required to explain the data.

2. EXPERIMENTAL

The series of ten experiments was carried out at Sandia's Shock Thermodynamics Applied Research (STAR) Facility. All ten tests made use of a single-stage powder gun with an 89-mm bore diameter. For the present series, either a low velocity of about 1.36 km/s or a high nominal velocity of 2.3 km/s (the maximum velocity of the gun) was used, as measured by electrical shorting pins with an accuracy of $\pm 0.5\%$. The impact planarity ("tilt") for this gun is typically less than 10 milliradians.

Experiments were performed in a forward-ballistics configuration, in which the sample was placed in a target and impacted by a flat plate to give rise to a planar shock wave with uniaxial loading and unloading on the time scale of the experiment (about 3 μs from shock arrival at the VISAR reading plane). A typical projectile-target design is shown in Figure 2.1. Parameters such as flyer and tamper/buffer thicknesses and materials were changed from shot to shot, as well as the presence or absence and thickness of LiF windows. The first test was with a baseline sample material: neoprene at solid density. The rest of the tests were done with powder samples pressed to 55% of TMD (theoretical maximum density). We use the term "tamper/buffer" plate because for some of the targets, a higher-impedance (tamper) plate was used while for others a lower-impedance (buffer) plate was used. The tamper plates were made of copper; the purpose was to reflect a strong compressive shock back into the sample. The buffer plates were made of the same material as the window (LiF). The purposes of the buffer plate were (1) to protect the thin layer of aluminum on the face of the window close to the sample (for the particle velocity measurement) and (2) to keep the geometry similar from one shot to the next. The specific parameters for each experiment are listed in Table 2.1 .

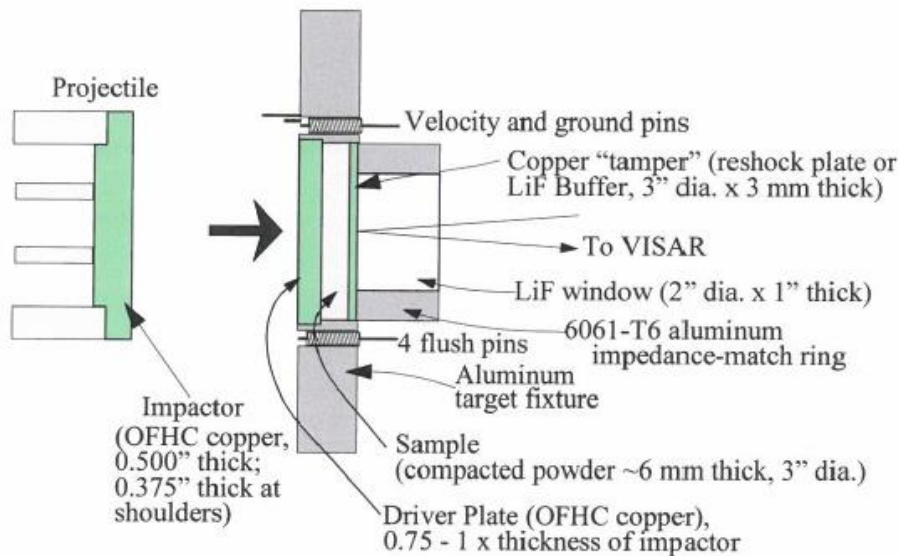


Figure 2.1 - Nominal projectile-target configuration. Details for each experiment are listed in Table 2.1 and Figs. 5.1-5.10.

Time-resolved particle-velocity histories for the first eight experiments were measured at the interface between the tamper/buffer plate and the window within each target using the laser velocity interferometry (VISAR) technique of Barker and Hollenbach (1972). In two experiments

(TWP-10, TWP-11) there was no window and the VISAR measurement was made at the free surface of the tamper plate. Data reduction was carried out using the VISAR93 code of Crawford (1993). In some experiments, two VISARs were used simultaneously to eliminate the ambiguity possible under rare circumstances when only one VISAR measurement is made. These tandem VISAR experiments also allowed us to assess the degree of lateral variation, giving us a measure of experimental uncertainty. The time intervals between impact and first motion at the VISAR recording surface were also obtained from the VISAR records, and are listed in the last column of Table 2.1. From these intervals, the transit times through driver and buffer materials can be subtracted to yield the sample transit times, from which shock velocities can be determined.

When new uncharacterized formulations were used, the mixing was done in ten-gram batches, and several batches of each material were combined to form a given lot. Each batch contained from two to four constituent materials, depending upon the mixture formulation. Those constituents having a propensity for agglomeration were sifted prior to mixing. In addition the constituents of each lot were mixed in a sequence chosen to achieve proper blending and safety. All mixing was accomplished by a rotary-action mixer for a fifteen-minute time period (Vandermolen et al.1994).

After the mixing operation, the powdered material was pressed into a target assembly designed for this test series. The pressing requirements to reach 55% TMD for each target differed depending upon the properties of the powder mixture used. The force varied from less than 1000 to greater than 6000 pounds. The material for each target was weighed to yield a finished product density of 55% TMD when pressed to a thickness of 6.00 ± 0.015 mm. The amount of material varied from 30 to 60 grams and was weighed out to an uncertainty of ± 0.1 mg (\pm about 0.0002% of the total weight). The buffer or tamper/ window assembly was inserted, and epoxied in place under a slight pressure. This subassembly was then transported to the STAR Facility, where the tilt and velocity pins were installed. The target was kept in an unheated storage facility until it was installed in the impact chamber of the powder gun. The target was destroyed during the experiment, and no pieces were recovered .

Table 2.1: Experimental Parameters

Exp.#	Date shot	Flyer material/ thickness (mm)	Driver material/ thickness (mm)	Sample material/ thickness (mm)	Nominal Sample density (% tmd)	Tamper/Buffer Material/ thickness (mm)	Window material/ thickness (mm)	Impact velocity (km/s)	Impact-to-signal time (μ s)
TWP-1	10/20/93	Cu/12.650	Cu/9.588	neoprene/5.55	100	LiF/3.252	LiF/25.426	2.303	3.14
TWP-2	10/25/93	Cu/12.530	Cu/9.592	RS234/6.0*	55	LiF/3.252	LiF/25.384	2.294	3.58
TWP-3	10/26/93	Cu/12.645	Cu/9.583	Al powdr/5.89	55	LiF/2.975	LiF/25.399	2.286	3.44
TWP-4	10/27/93	Cu/12.657	Cu/9.596	RS234/5.932	55	Cu/3.208	LiF/25.422	2.285	3.80
TWP-6	11/15/93	Cu/12.642	Cu/9.566	GA134/6.00*	55	LiF/3.175*	LiF/25.4*	2.267	3.67
TWP-7	11/17/93	Cu/15.846	Cu/9.552	RS234/6.038	55	Cu/1.062 LiF/3.266	LiF/25.436	1.356	4.96
TWP-8	11/19/93	Cu/15.826	Cu/9.542	CS691/5.975	55	Cu/1.032	LiF/25.432	1.364	4.50
TWP-9	11/22/93	Cu/15.875	Cu/9.561	CO104/6.00*	55	LiF/3.094	LiF/25.424	1.367	4.97
TWP-10	11/29/93	Cu/15.815	Cu/9.562	RS234/6.114	55	Cu/1.003	no window	1.374	4.44
TWP-11	4/25/94	Cu/15.850	Cu/9.572	RS234/5.938	55	Cu/1.010	no window	2.209	3.42

*Nominal value

3. COMPUTATIONAL

We modified the CTH hydrocode (McGlaun et al. 1990) for the simulation of the reactive powders tested in the work described in this report. The modifications included installation of a new equation of state and reaction law. These modifications will be described briefly here. The model was developed primarily as a means of simulating applications of this class of reactive materials. It has also found use in the design and interpretation of shock wave experiments, as is shown in this report.

The equation of state is mechanical in nature; it provides a relation of the form $P(V, \lambda)$ where P is pressure, V is specific volume, and λ is the reaction parameter (fraction of reacted material, $0 \leq \lambda \leq 1$). Pressure-volume and pressure-compression curves (compression μ is defined by $\mu = (V/V_0) - 1$ where V_0 is the specific volume at the reference density ρ_0) are shown schematically in Figure 3.1. A mechanical equation of state (one that does not include any explicit dependence on temperature) is justified in cases where there is only one thermodynamic path of interest, e.g. compression of the reactant along the Rayleigh line followed by isentropic expansion of the product. In such cases, we may take advantage of the great simplification achieved by neglect of the temperature dependence, provided we remember that the pressure-volume curves correspond to this particular thermodynamic path. However, as we shall see, such a purely mechanical equation of state is insufficient to reproduce the loading and release behavior of the highly porous solids used in the present study. Future modeling of such solids will need to take into account both irreversible heating due to pore compaction, and the heterogeneous nature of energy deposition which can result in phase changes.

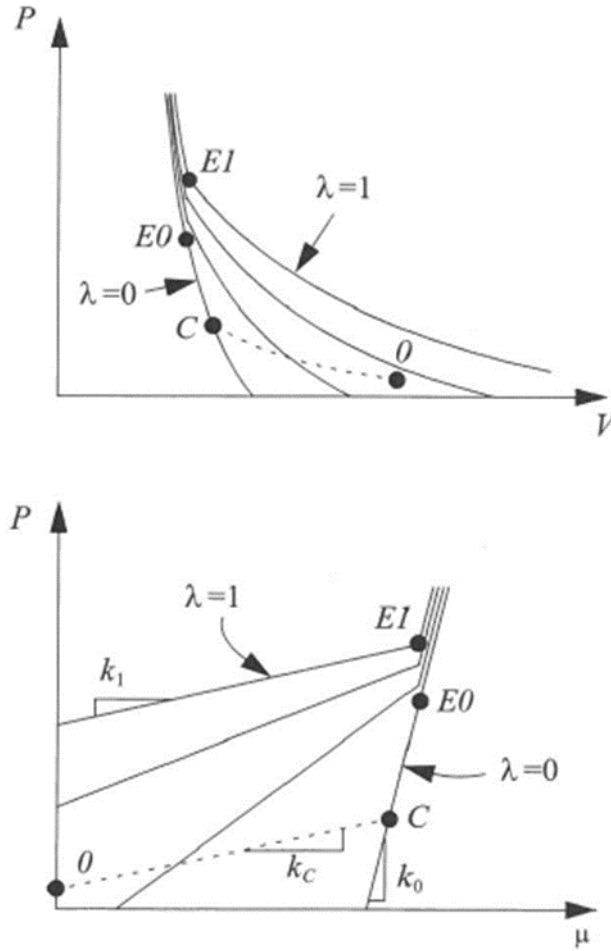


Figure 3.1 - Pressure-volume curves (top) and a pressure-compression curves (bottom) for four values of A . in the CTH model. The segment OC represents partially crushed reactant.

A central assumption in the present equation of state is that there is a value of compression μ_E which separates qualitatively solid-like and gas-like behavior in the product. As shown in Figure 3.1, the response in each of these regimes is represented by straight lines in P - μ space. In the case of reactant ($\lambda=0$), the slopes of these lines coincide, since the reactant is a solid.

If k_0 and k_1 are the slopes of the lines in the gas-like regime for reactant ($\lambda=0$) and product ($\lambda=1$) respectively, the slope at any intermediate value of λ is found from

$$k(\lambda) = k_0 + (k_1 - k_0)\lambda^m \quad , \quad \mathbf{3.1}$$

Where m is a positive constant. The pressure at compression μ_E for intermediate values of λ is found from

$$P_E(\lambda) = P_{E0} + (P_{E1} - P_{E0})\lambda \quad . \quad \mathbf{3.2}$$

Observe from Figure 3.1 that even if reacted or partially reacted material is in the solid-like regime ($\mu > \mu_E$), there is an increase in volume at constant pressure. Thus, there is some mechanical difference between reacted and unreacted material at any value of compression, but the difference is more pronounced at low compression (high volume).

It is known that, as a porous solid crushes within a shock wave, dynamic effects cause it to experience positive pressure prior to total crushing out of all the pore space. (This implies that the solid is not in mechanical equilibrium with the voids, which have zero pressure.) We assume that the partially crushed behavior is represented by the straight line in P- μ space shown by the dashed line in Figure 3.1. In applications of interest, usually crushup (removal of all the pores) occurs in the model prior to any reaction or unloading. However, the model has the capability to represent unloading from partially crushed states at any value of λ . In such cases, unloading occurs from the dashed line in Figure 3.1 along a line with slope $k(\lambda)$ given by Equation (3.1).

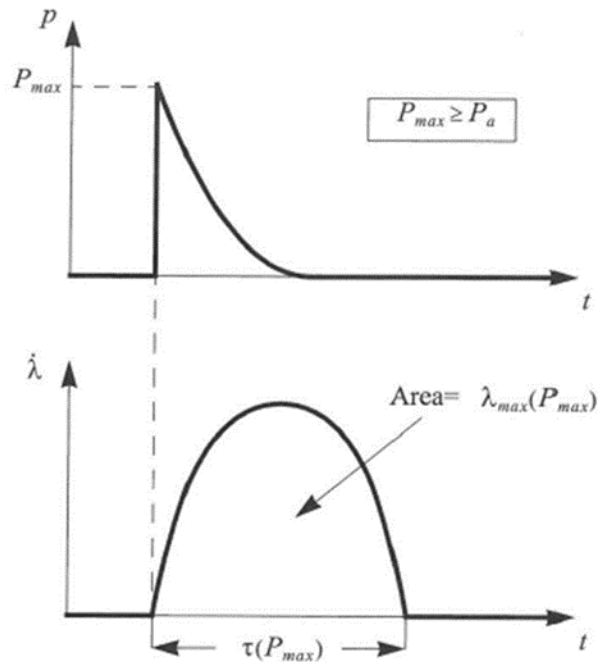


Figure 3.2 - Reaction kinetics model. Top: pressure history at a point, showing a shock wave. Bottom: reaction rate history at the point.

The reaction kinetics model computes $\lambda(t)$ based on the maximum pressure, P_{max} , that is experienced locally at a material point. The model is illustrated in Figure 3.2. The maximum extent of reaction at a point, λ_{max} , is determined as a piecewise linear function of P_{max} , as shown in Figure 3.3. The constant P_a , known as the initiation pressure, is the lowest pressure which causes a reaction to occur. The reaction goes to completion if the maximum pressure exceeds another constant, P_b . The reaction time, τ , is also a piecewise linear function of P_{max} , as shown in Figure 3.4. This dependence is motivated by the assumption that higher shock pressures result in faster reactions.

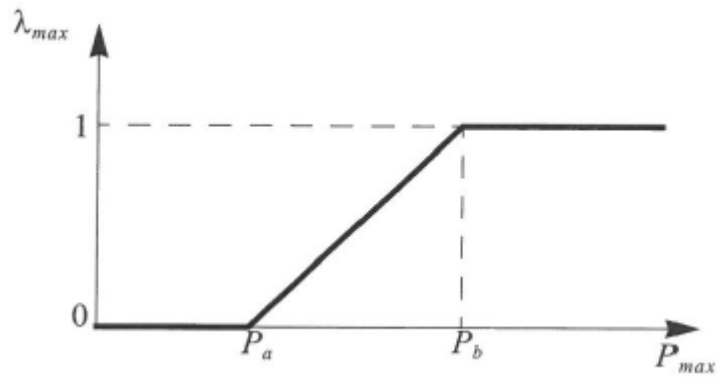


Figure 3.3 - Determination of maximum extent of reaction.

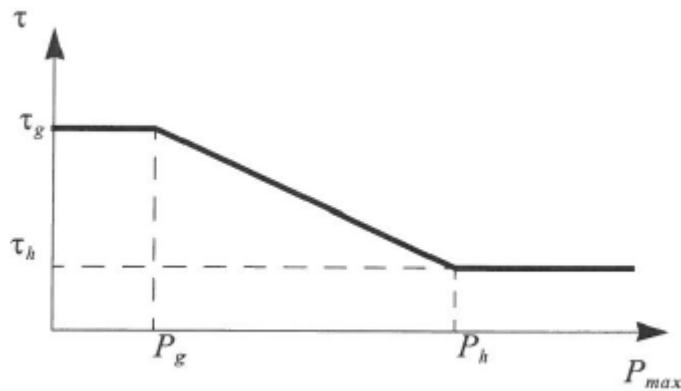


Figure 3.4 - Reaction time as a function of maximum pressure.

Table 3.1: Numerical Parameters

Parameter	Value
k_{E0}	5.71×10^{10} Pa
k_{E1}	1.09×10^{10} Pa
k_C	6.84×10^9 Pa
V_0	5.85×10^{-4} m ³ /kg
m	0.3
μ_E	1.0893
P_0	1.0×10^5 Pa
P_{E0}	1.5×10^{10} Pa
P_{E1}	2.0×10^{10} Pa
P_a	2.0×10^9 Pa
P_b	3.0×10^{10} Pa
P_g	9.0×10^9 Pa
P_h	5.0×10^{10} Pa
τ_g	5.0×10^{-6} s
τ_h	5.0×10^{-6} s

4. RESULTS AND DISCUSSION

The basic experiment is depicted schematically in Figure 4.1, which shows the configuration, Hugoniot analysis, and particle-velocity data for experiment TWP-2, the first of our experiments on RS234 powder. The Hugoniot analysis is pictured in the plot of pressure (P) versus particle velocity (u) in the upper left of Figure 4.1. The powder mixture components are defined by Vandermolen et al. (1993). The exact values of various parameters that were measured are given in Table 2.1; nominal values are given in the following description.

The 6-mm-thick sample was sandwiched between a 9.6-mm-thick copper driver plate and a 3.25-mm-thick LiF tamper. A thick (12.65 mm) copper flyer plate impacted at about 2.3 km/s, driving an approximately 15-GPa shock into the powder. The state behind this first shock wave can be inferred independently of the measured particle velocity by performing an impedance-match solution (Rice et al. 1958) using the mean shock velocity, determined by dividing the initial sample thickness by transit time. The transit time comes from the known time of impact, the known thickness and shock velocities in the copper driver and LiF tamper, and the measured time of arrival of the first shock wave at the tamper-window interface (the velocity histories shown in Figure 4.1 and subsequent figures are time-shifted so that the first arrival corresponds to time $t = 0$; time intervals between impact and arrival at the reading location are listed in Table 2.1). In all cases, impedance matching leads to self-consistent solutions as expected for the steady or near-steady waves that were generated in the experiments.

In TWP-2, the sample reverberated up to a maximum pressure by successive shock reflections off the bounding surfaces and reached a peak state "F" (for "final" state), approximated by the intersection of the recentered copper and LiF Hugoniots, with a particle velocity of approximately 1.6 km/s. After about 3 μ s, the particle velocity began to drop due to the arrival of a rarefaction wave from the back side of the flyer plate. The window thickness was large enough that there were no rarefactions from the downstream side of the sample, and the large diameter prevented edge rarefactions, so the strain was uniaxial until this point in time. At about 3.5 μ s, there was a sharp arrival in the experimental velocity data. We believe that this was due to the fact that the tensile stress exceeded the spall strength of the copper flyer along the center line, but not along the radius supported from behind by a phenolic cylinder (see Figure 3.1). This caused a spall plane of finite lateral extent to open and suddenly close, generating a shock wave which propagated through the sample. The arrival of this shock at the tamper-window interface marks the end of useful data, because it depends on two-dimensional effects. For the same reason, its presence was not predicted by the one-dimensional code calculations.

Using the same format as in Figure 4.1, the test configuration, Hugoniot analysis, and particle velocity history are shown for each of the other experiments in Figures 4.2 through 4.10. For the RS234 experiments the calculated as well as the measured particle velocity histories are shown. For the other powder formulations only the measured particle velocity is shown.

Experiment TWP-2 (RS234)

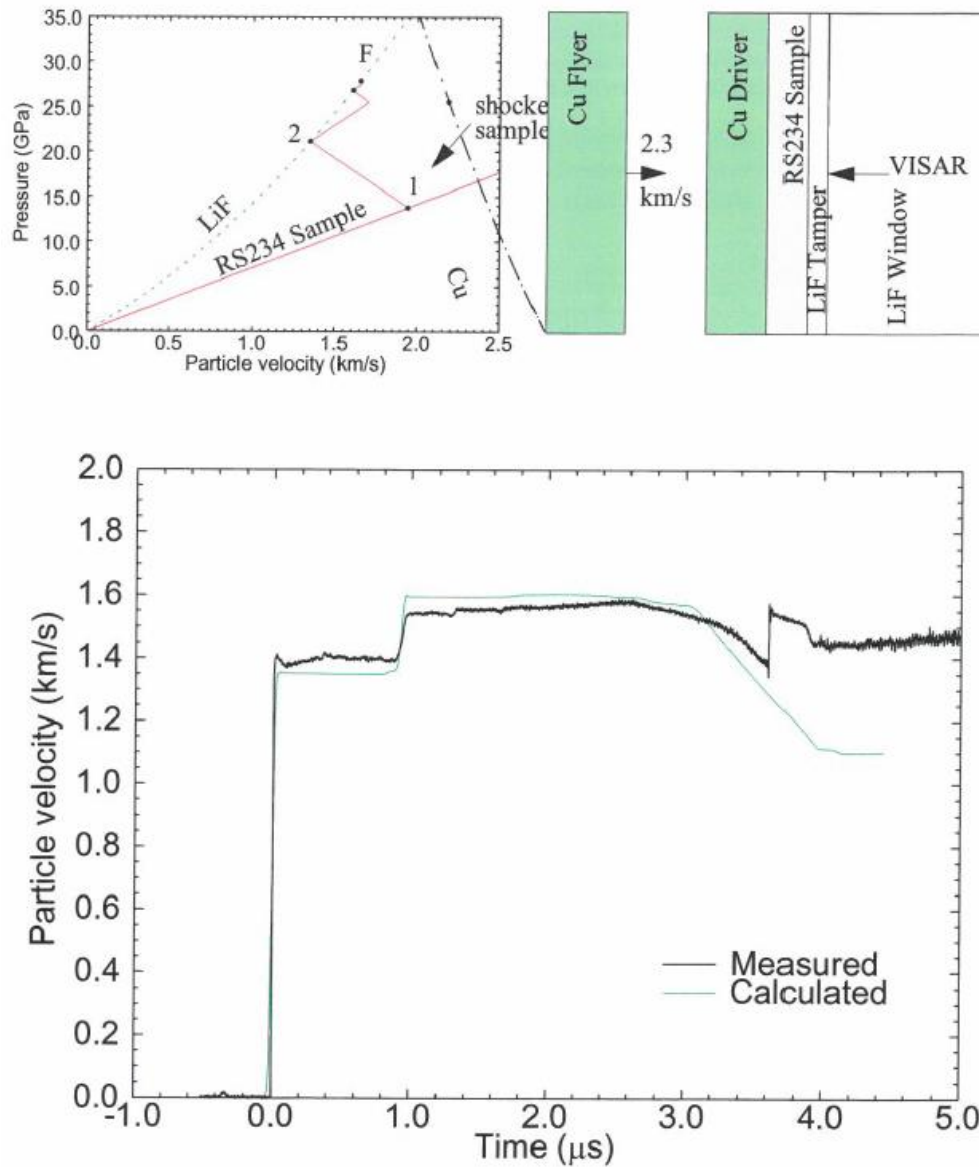


Figure 4.1 - Schematic P-u diagram and experimental configuration for experiment TWP-2 (RS234). Bottom : Measured particle velocity history at point indicated in upper right-hand corner, and CTH prediction of particle velocity history using inert model.

Experiment TWP-1 (Neoprene)

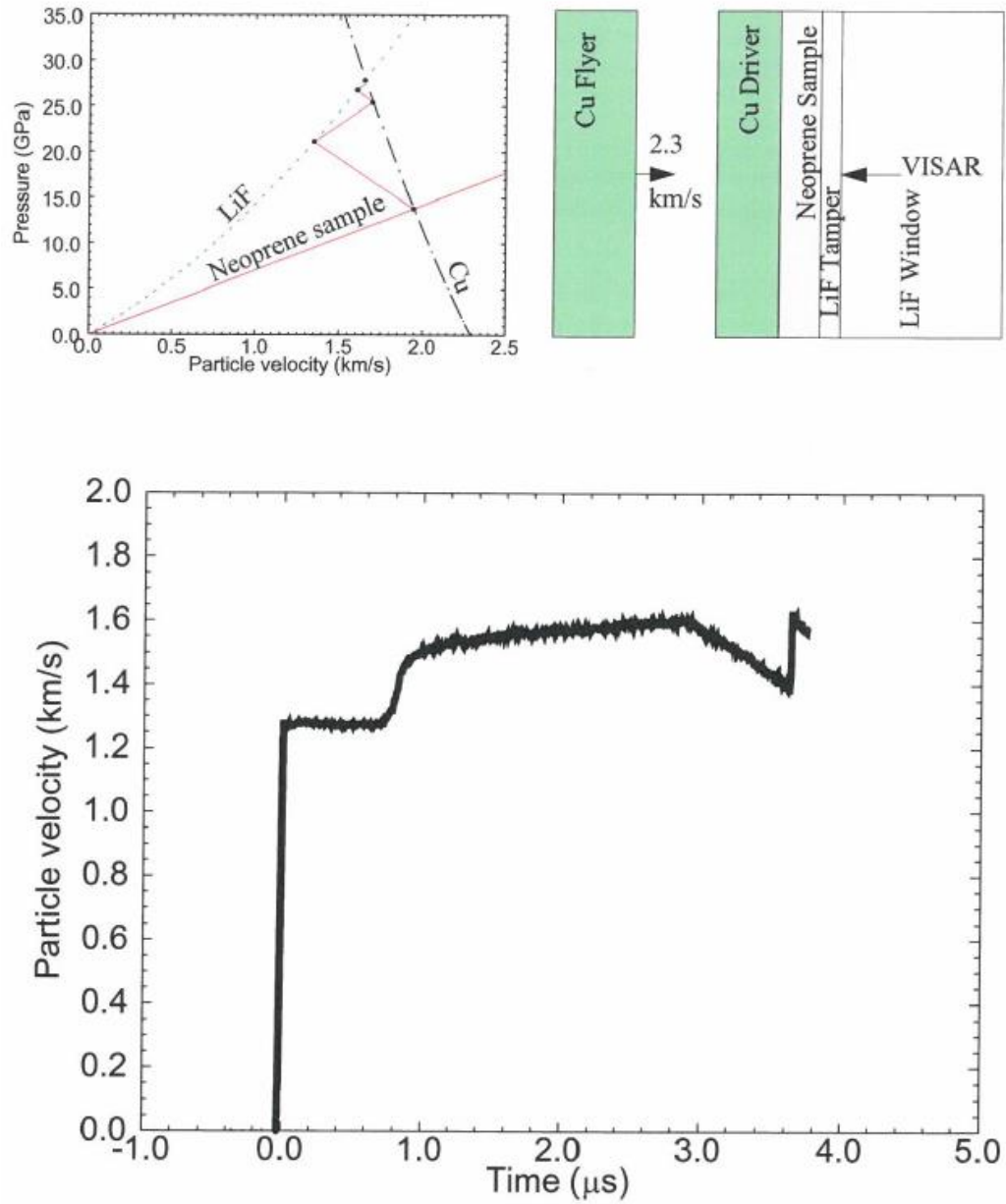


Figure 4.2 - TWP (neoprene) data, displayed as in Fig. 4.1

Experiment TWP-3 (Aluminum powder)

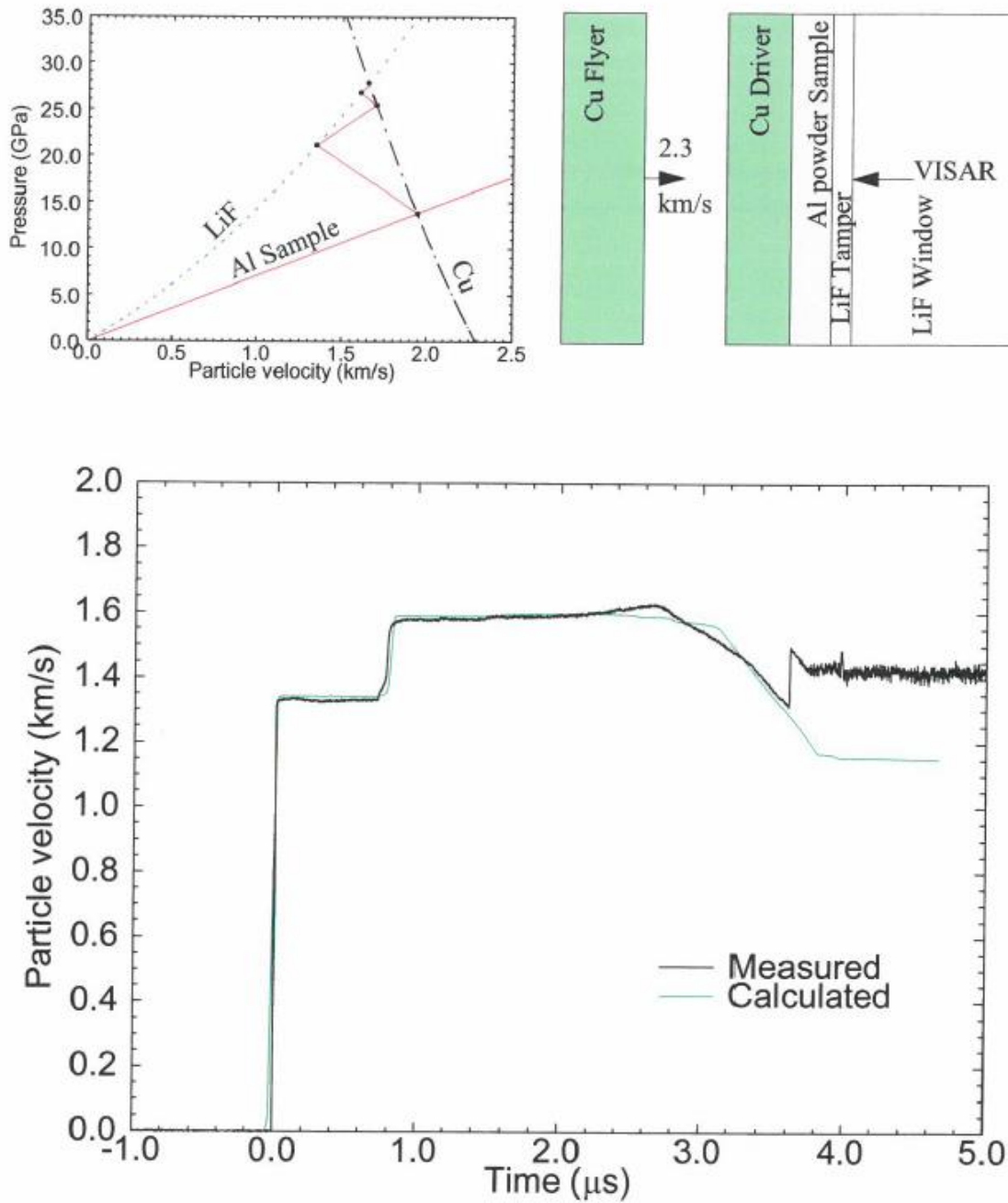


Figure 4.3 – TWP-3 (Aluminum, powder) data.

Experiment TWP-6 (GA135)

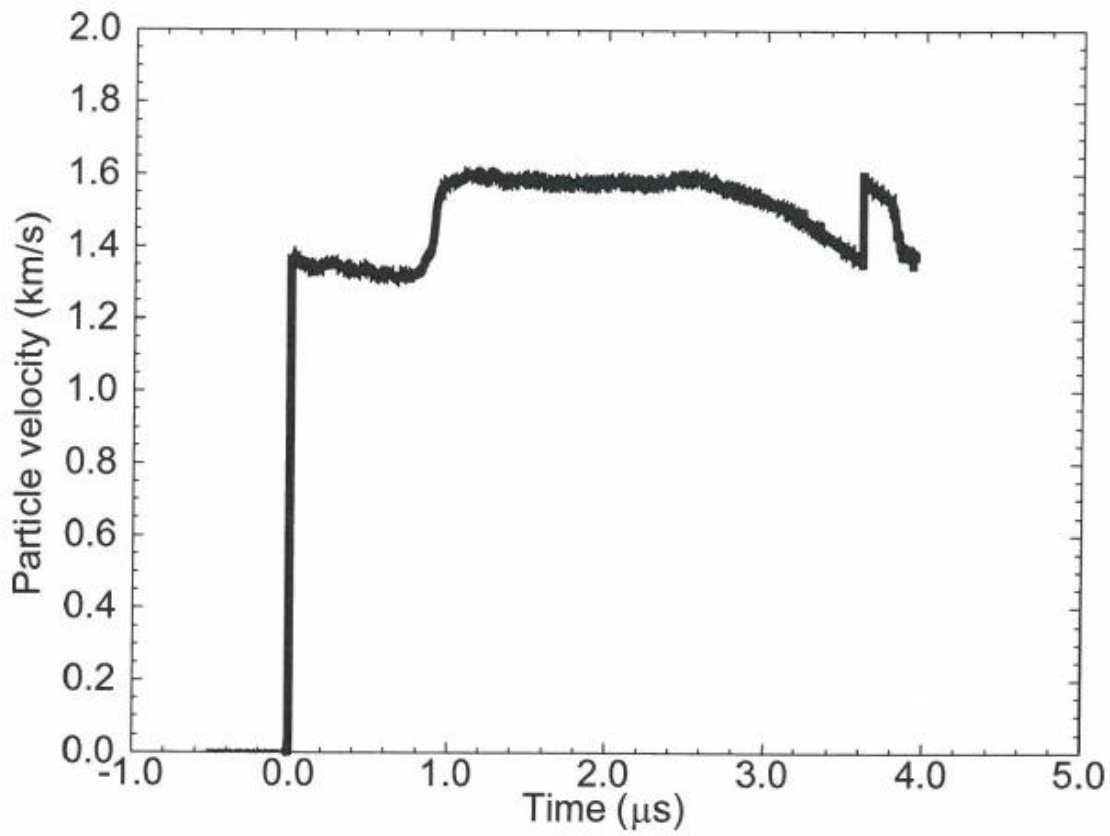
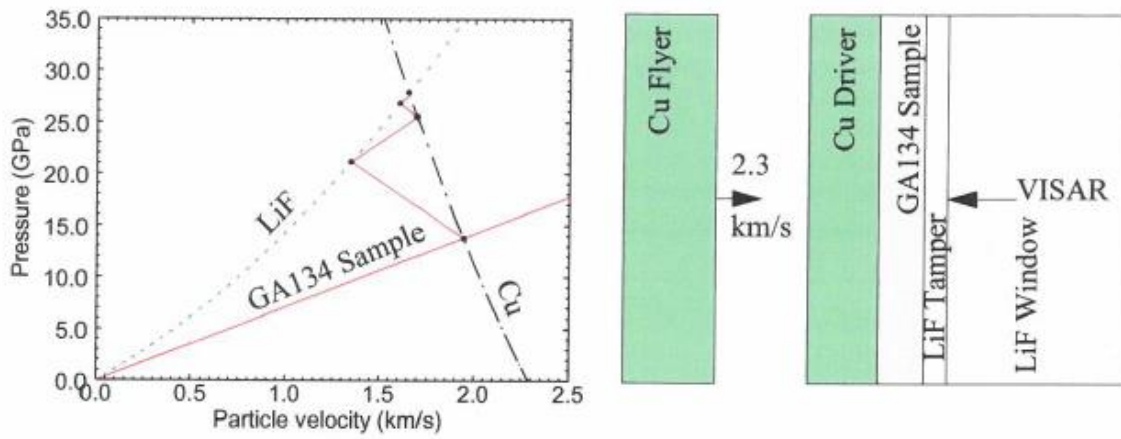


Figure 4.4 – TWP-6 (GA134) data.

Experiment TWP-9 (CO104)

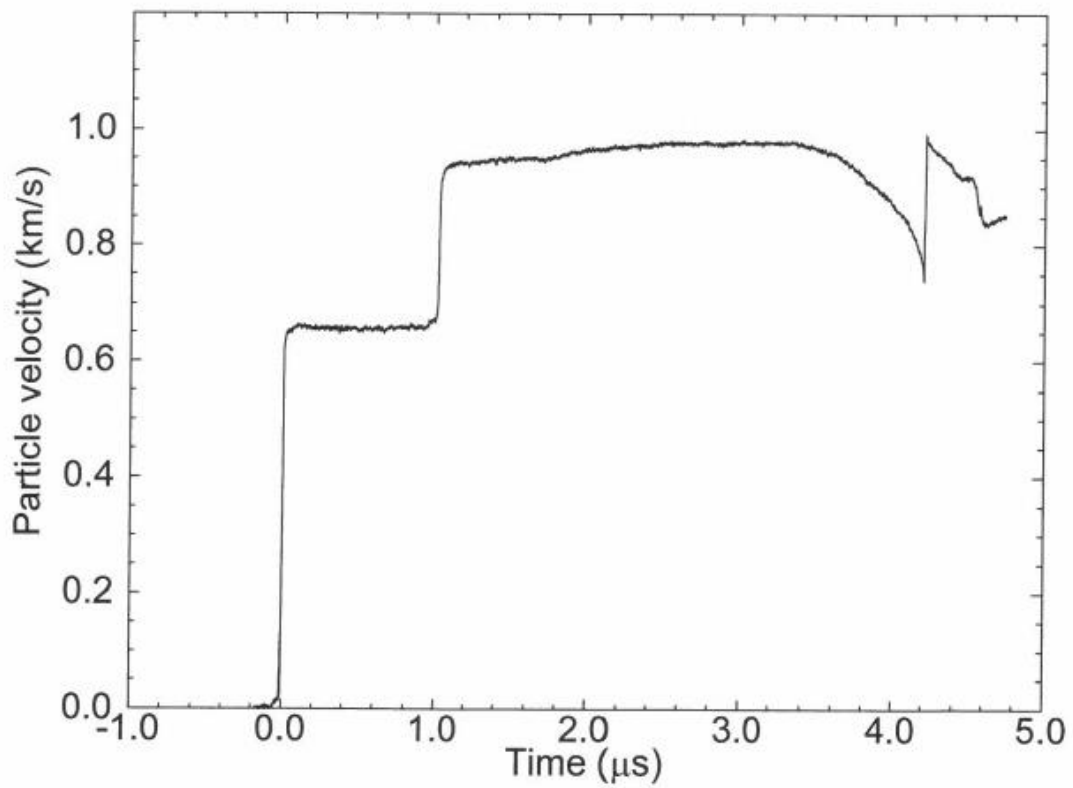
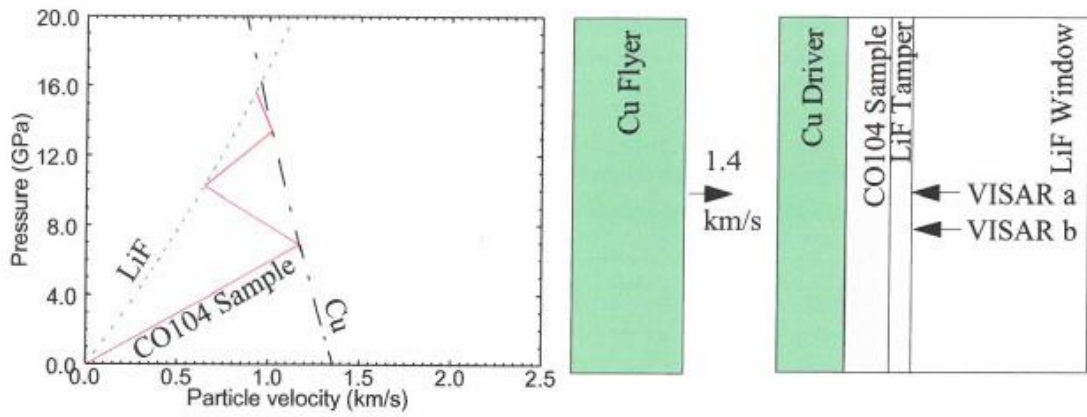


Figure 4.5 – TWP-9 (C0104) data.

Experiment TWP-4 (RS234)

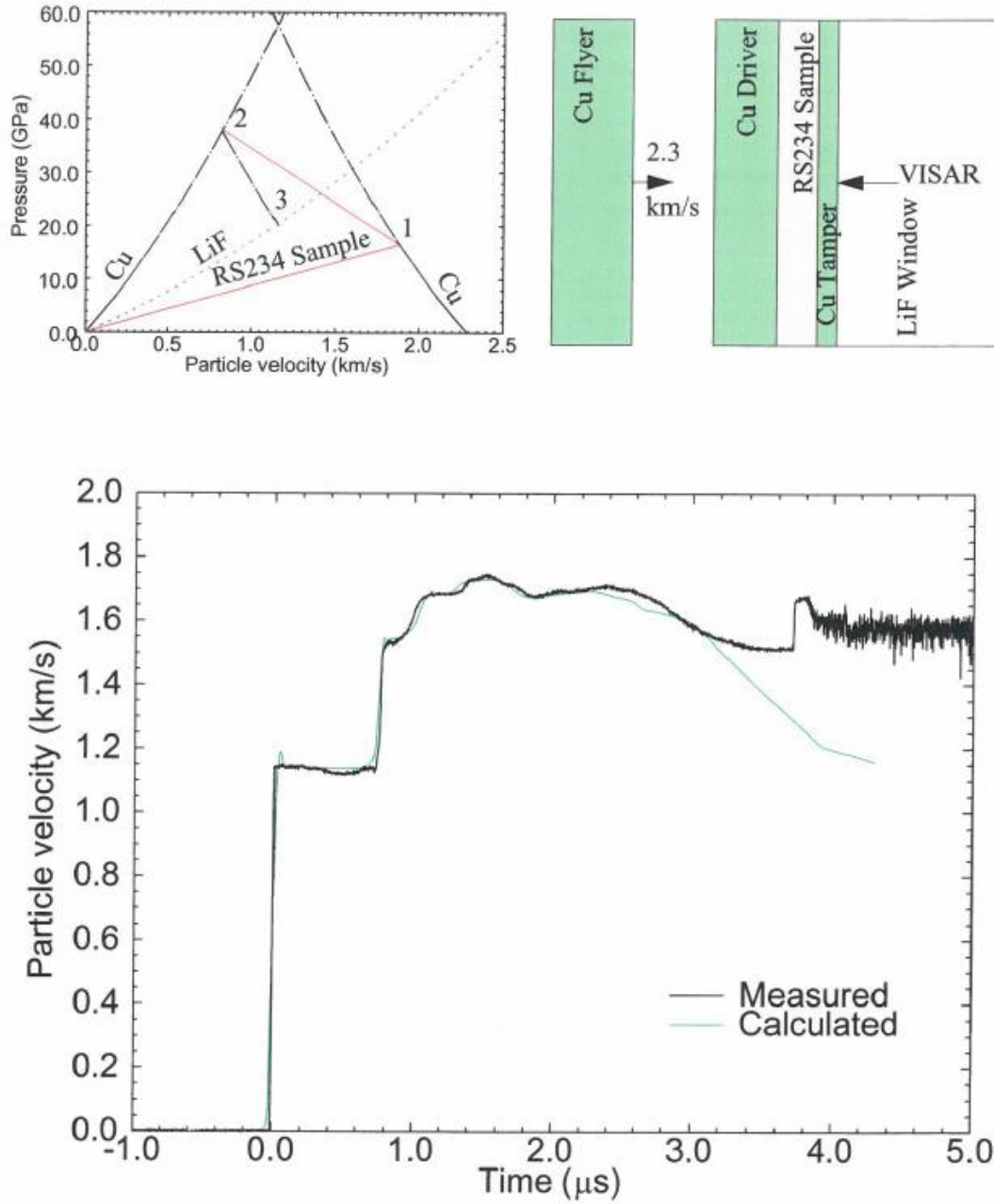


Figure 4.6 – TWP-4 (RS234) data

Experiment TWP-7 (RS234)

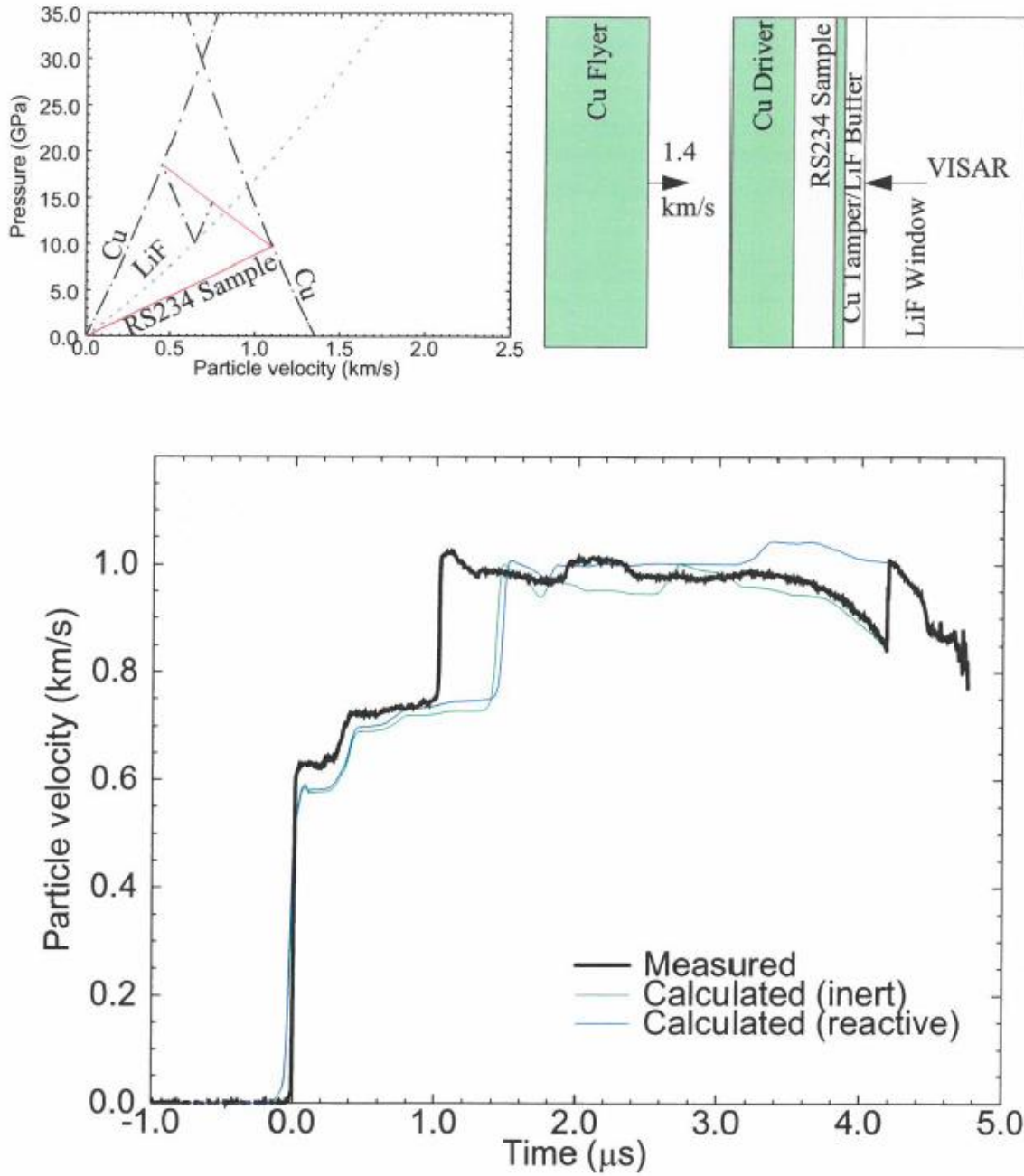


Figure 4.7 - TWP-7 (RS234) data, with two calculated velocity histories, one with an inert model and one with a reactive model.

Experiment TWP-8 (CS691)

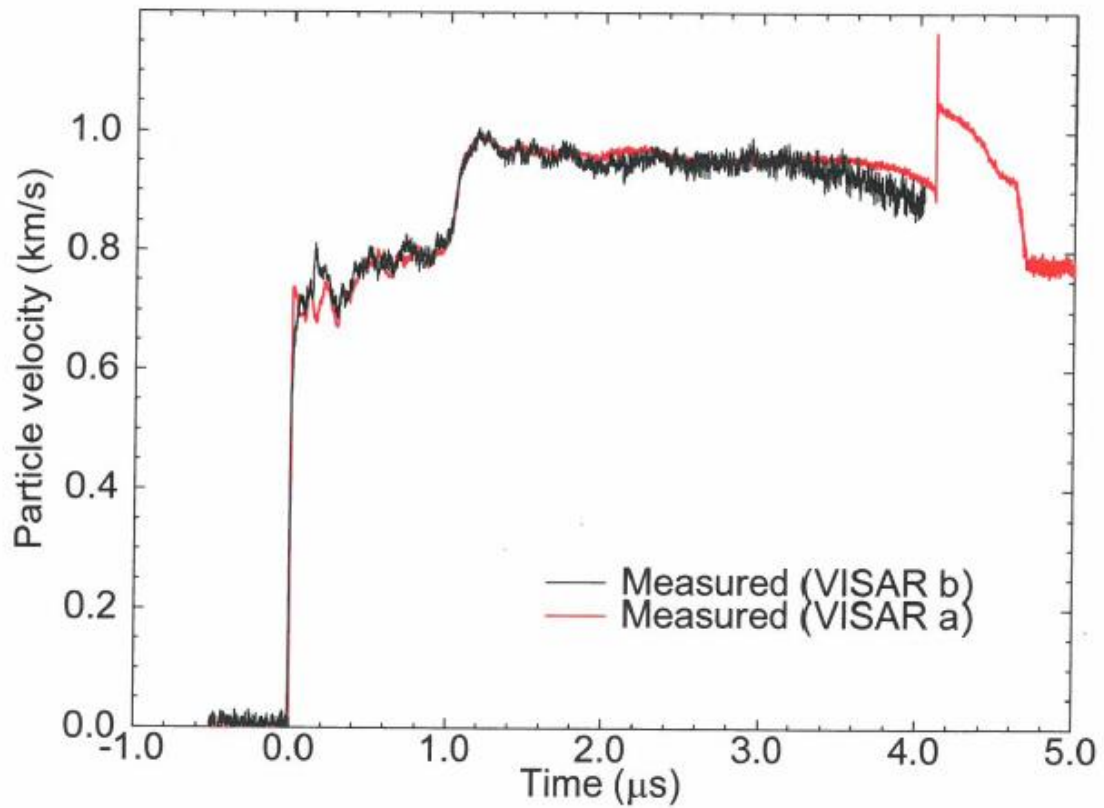
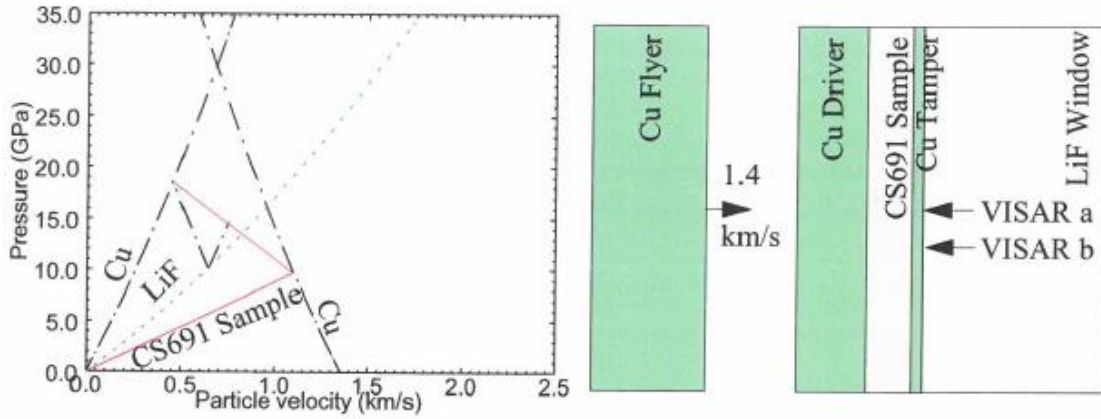


Figure 4.8 - TWP-8 (CS691) data. Two independent velocity measurements are shown.

Experiment TWP-10 (RS234)

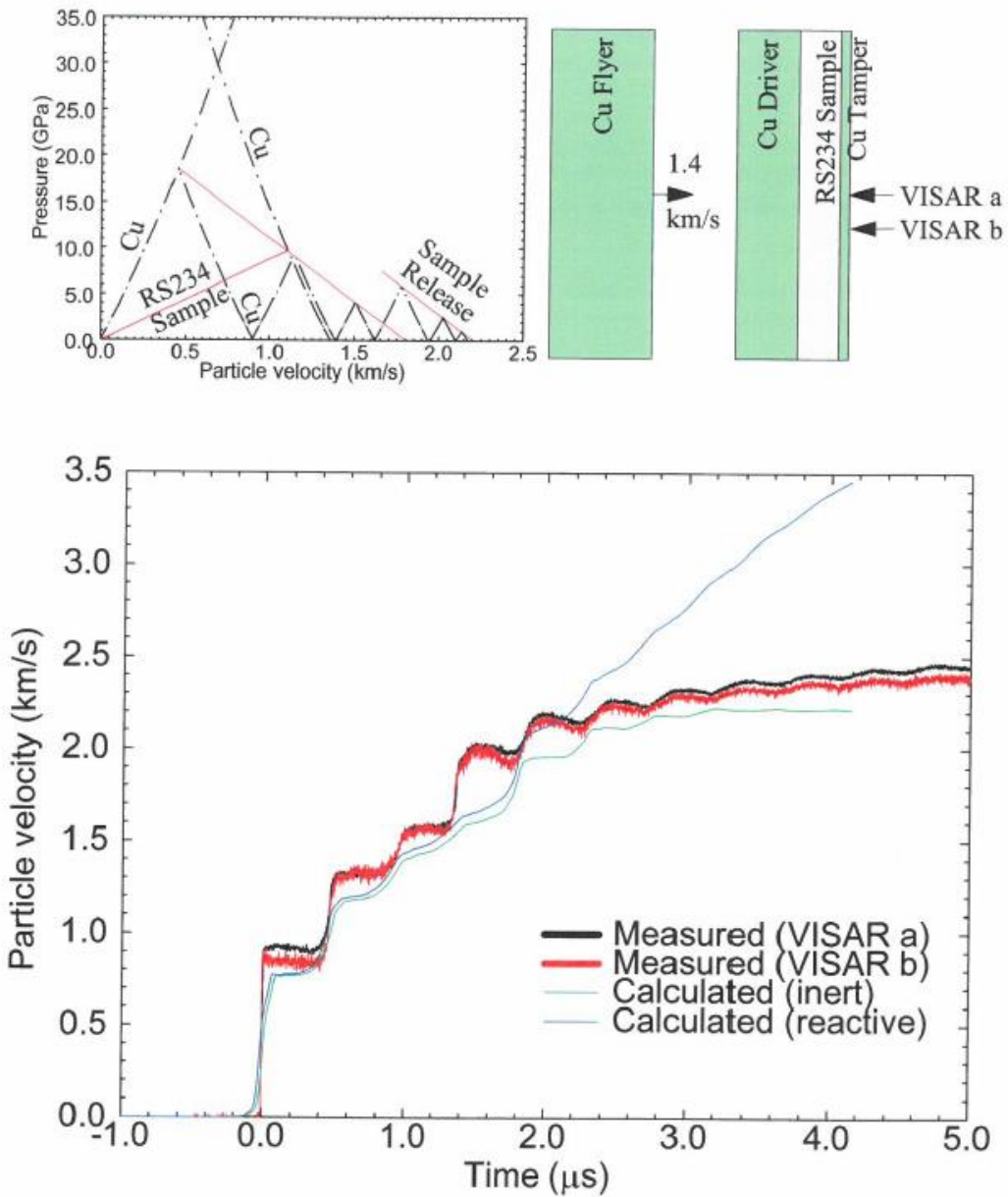


Figure 4.9 - TWP-10 (RS234) data. Two independent free-surface velocity measurements are shown along with inert and reactive calculated velocities.

Experiment TWP-11 (RS234)

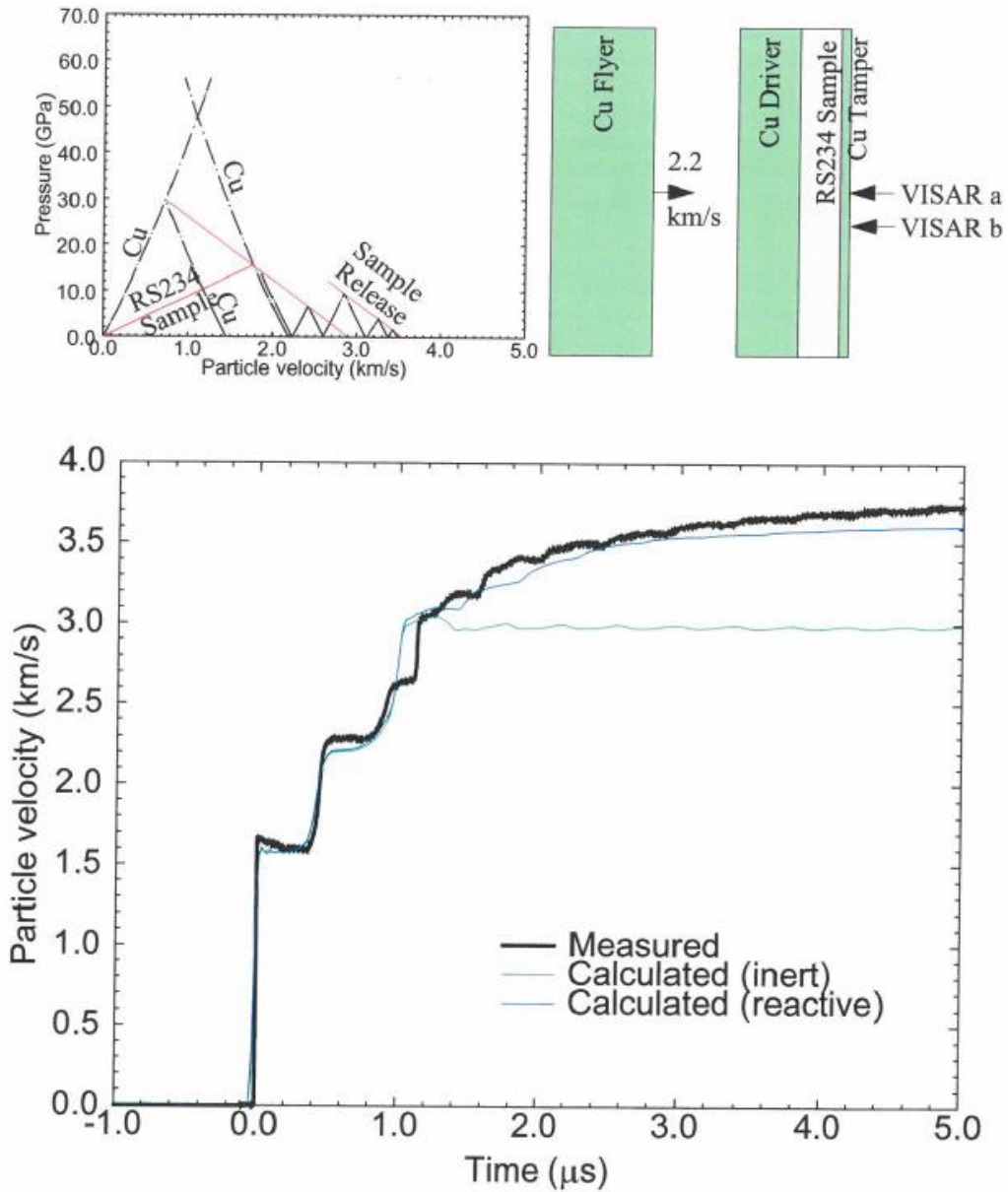


Figure 4.10 – TWP-11 (RS234) data

As mentioned in the introduction, two control experiments were performed under almost identical conditions and showed very similar time-dependent behavior. Figures 4.2 and 4.3 show the data on neoprene and on 55% TMD aluminum powder, respectively. In both experiments, the first observed state does not change significantly with time over a period of about 0.5 μ s. However, the particle velocity associated with the second observed state increases by as much as 5% over its approximately 2 μ s duration in both cases, indicating that a time-dependent relaxation is taking place. A detailed discussion of the causes of the relaxation in aluminum powder is beyond the scope of this report. It could represent any viscoelastic, -plastic or thermal time-dependent phenomena, having nothing to do with chemical reactions, that return the shocked material to thermal and/or mechanical equilibrium. These control experiments illustrate the magnitude of time-dependent behavior that can take place under experimental conditions in which we know there are no chemical reactions between components.

Although there are many similarities between the velocity histories of the two control experiments, there are also some differences, most evident in the way the particle velocity increases until the sharp drop occurs at about 3 μ s. Looking at the particle-velocity trace for the porous aluminum target (Figure 4.3), one can see that the particle velocity stays constant after the second jump for about a microsecond. The increase for the neoprene experiment (Figure 4.2) starts earlier and may be due to different processes.

The fact that the measured velocity in TWP-2 and some other experiments is not constant between the first two arrivals is consistent with a powder that is not of perfectly uniform density. CTH calculations were run on a powder with a density that varied through its thickness, and similar behavior was predicted. It is tempting to attribute the gradual increase in particle velocity after the second arrival to chemical reaction. However, a change of this magnitude can also be explained by time-dependent effects such as those listed above. In fact the two control experiments both give rise to stronger rate effects than observed in TWP-2. The difference between predicted and measured velocity values in experiment TWP-2 is attributable to uncertainty in equation-of-state parameters used for the powder mixture in the CTH calculation and the fact that thermal effects were neglected.

In Figures 4.4 and 4.5, data are shown from experiments on two new compositions, GA134 and CO104. Both tests were performed using the same experimental configuration as for TWP-2. The GAJ 34 (TWP-6) was shot at the same high velocity, but for the CO104 shot (TWP-9) a lower impact velocity was chosen to investigate the possibility that any reaction is inhibited by the higher pressures experienced in the earlier tests. In TWP-9 and several other experiments (see Table 2.1), a thicker flyer plate was used to delay the arrival of the rarefaction wave and increase the length of time available for collection of useful (one-dimensional) data. This is evident in the data as a delay in the inferred spall signature. In both experiments on the new formulations, strong increases in particle velocity (or, by inference, pressure) were not observed.

In experiments TWP-4, TWP-7, and TWP-8, copper tampers were used to achieve higher peak shock pressures for a given impact velocity, and to provide partial release states in order to allow determination of possible vapor production. In Figure 4.6, the loading history can be visualized schematically from the pressure/particle-velocity diagram. The first shock state (1) is determined only by the impact conditions, and is about the same as that of TWP-2 (Figure 4.1). The second

shock state (2), is at much higher pressure, because the shock has reflected off of the copper tamper, which is a higher impedance material than the LiF buffer used on TWP-2. The particle velocity associated with state 3 (see Fig. 4.6) is that which is directly measured at the tamper/window interface, and is a partial-release state in copper, from which state 2 can be inferred. It is from the second measured state that the partial-release path of the powder can be determined. If a strong reaction produced highly compressible gaseous products at high temperature, it would have a very shallow release path (small slope in the P-u plane) compared to that of unreacted and unvaporized powder which remains condensed and relatively incompressible. Unreacted powders which undergo a small amount of inhomogeneous vaporization would have an intermediate release path. The second-particle velocity jump and subsequent history should thus be highly dependent on the extent of reaction.

After the second jump, it is difficult to use the P-u diagram to track states because of multiple shock interactions with shocks reflected from the driver plate. It becomes necessary to rely fully on the CTH simulations. As can be seen in Figure 4.6, the measured particle velocity history after this point in time is almost identical to the calculated history assuming no reaction, until the release wave effects begin to dominate after about 3 μ s.

Another experiment (TWP-7) using the same geometry, but with a lower impact velocity, was performed on RS234, again to investigate the possibility of high pressure inhibiting the reaction rate in TWP-4. The large jump in particle velocity about 1 μ s after first arrival is the first reflection from the driver-powder interface. The pressure/particle-velocity diagram (Figure 4.7) is qualitatively the same as for TWP-4, but the pressures and particle velocities are lower. The VISAR measurement from TWP-7 does not agree as well with the calculations as for TWP-4. A trend is evident from experiments TWP-2, TWP-4, and TWP-7, in that the error in the calculated velocity of the first jump becomes progressively larger for lower shock pressures. This is most likely due to that fact that the very different thermal components in pressure are ignored by the purely mechanical equation of state. A mechanical equation of state that is optimized to reproduce a velocity history for a given experiment in which there is a large thermal component will not be stiff enough to match data at lower pressure. The same equation of state that appears to provide a very good match to the data for TWP-4 falls short for TWP-7, where the experimental shock and particle velocities are much higher than predicted. Both the inert and reactive calculations yield similar results because the shock pressures are below the threshold for significant reaction by the reactive model.

Experiment TWP-8 was a test of another new mixture, CS691. It was nearly identical to TWP-7 but with the addition of a second VISAR. In Figure 4.8 the results of both VISAR measurements are plotted, showing a high degree of consistency. The "noisier" nature of the velocity history may have been due to a less homogeneous compact than the one used in TWP-4.

We performed two tests, TWP-10 and TWP-11, in a "ring-down" (windowless) geometry to investigate the release path of the sample material to lower pressures, where the effects of any gas-producing reaction should be greatest. The pressure/particle-velocity diagrams in Figures 4.9 and 4.10 show the sequence of states experienced by the samples, and how they are related to the particle-velocity history of the free surface, which was measured. The release path of the sample provides the upper "envelope" beneath which the copper tamper plate reverberates in the P-u plane. For a very thick sample, the final ring-down state would be determined by a single release path;

but because of a shock reflection from the driver a second release increases the final particle velocity to a higher value. This is also the cause of the larger jump in particle velocity seen in the data for the fourth arrival. For compressible (and expandable) reaction products, the release path that bounds the ringing copper plate from above will be shallow and will intersect the zero pressure axis at a higher particle velocity than it would if it were a steep path, as it would be for a mixture of unreacted condensed material. In other words, a strong vapor-producing reaction would accelerate the thin copper plate to a much higher velocity than it would reach otherwise.

Close examination of the VISAR measurements in both TWP-10 and -11 show that the velocity continues to increase. This implies that the release path has not yet reached zero pressure as the particle velocity increases. Therefore, the release path becomes shallower at low pressure indicating the presence of some vapor. However, real-time pyrometric measurements of coarse powders have shown that the temperature distributions can be quite heterogeneous following shock loading (Boslough 1992b, Yoshida, 1994). Local temperatures can greatly exceed the vaporization temperature of the powder, even though the mean bulk temperature (the temperature that would be achieved upon thermal equilibrium) does not. Under these circumstances, heterogeneous vaporization upon release would result, giving rise to a continuously increasing free-surface velocity as observed.

In principle, the difference between the final velocity of the plate can be compared to its predicted value to get an upper bound on work output due either to heterogeneous vaporization or any reaction. However, for experiment TWP-10, the relative difference at late time between the inert model and the experimental data is similar to that for the first shock state. This implies that the difference in particle velocity at late time can probably be attributed primarily to the degree of inadequacy of the equation-of-state model. The reactive model appears to agree quite well with the data for TWP-11, but careful examination shows that it fails to reproduce the behavior of the sample at early times. While the agreement of the model at late times is indicative of vapor production upon pressure release, it is not necessarily an accurate representation of the shocked material. Before coming to any conclusions as to whether a reaction took place in this experiment, control experiments on each individual component of the mixture are required to rule out the possibility of vapor production by other means.

As mentioned earlier, the boundary condition between the sample and driver allows an impedance-match solution (Rice et al. 1958) with the known copper Hugoniot centered at the impact velocity for a full description of the shock state of the powder. In this state, indicated by "1" in Figure 4.1, the pressure P_1 , density ρ_1 , shock velocity U_1 , and particle velocity u_1 are all known. There is, however, some uncertainty associated with this state because of the required assumption that the first shock is a steady (constant-velocity) wave. This assumption is probably a good one for an inert powder under the conditions of these experiments with a single input shock, but for a strongly reactive sample it is possible that it could be in error. The fact that this analysis leads to self-consistency is evidence for its validity. The shock velocities, pressures, particle velocities, densities, and relative specific volumes determined in this way for the first shock state are listed for all the RS234 experiments in Table 4.1. Uncertainties were determined by standard methods based on conservative estimates in measurement error of initial sample density, impact velocity, and shock velocity.

The control experiment on neoprene (TWP-1) provides an independent confirmation of this experimental method. The measured time interval Δt_{tot} between impact and shock arrival at the back of the buffer was 3.144 μs . Because the impact is symmetric (copper-on-copper), the particle velocity in the driver is exactly half the measured impact velocity. The shock velocity in the copper driver comes directly from its known Hugoniot; dividing this into its thickness (Table 2.1) yields its shock transit time Δt_d . For the LiF buffer, the particle velocity of the first shock state was directly measured by the VISAR. The buffer shock transit time Δt_b is determined the same way as for the driver. The transit time through the sample is simply the difference $\Delta t_s = \Delta t_{tot} - \Delta t_d - \Delta t_b$. For experiment TWP-1, $\Delta t_s = 0.97 \mu\text{s}$, and $U = d_s / \Delta t_s = 5.55 \text{ mm} / 0.97 \mu\text{s} = 5.72 \text{ km/s}$. This experimental shock velocity is less than 4% greater than the value calculated for these loading conditions using the neoprene Hugoniot from Marsh (1980). Timing errors associated with the experiments on powders are expected to lead to proportionately smaller relative uncertainties, because the shock velocities are lower (see Table 4.1).

A description of the second (reshock) state in the sample comes directly from the particle-velocity measurement. When the first shock reaches the LiF buffer, a shock is reflected back into the sample and another travels through the buffer and into the window where the particle velocity jumps to about 1.4 km/s. The known Hugoniot of LiF uniquely determines the P-u state, which must be the same in the sample due to the boundary condition. This is state "2" in Figure 4.1. All the relevant parameters were determined for this reshock state for all the experiments using the following equations:

$$U_2 = \frac{1}{\rho_1} \left(\frac{P_2 - P_1}{u_2 - u_1} \right) \quad , \quad (4.1)$$

$$\rho_2 = \rho_1 \left(\frac{U_2}{U_2 + u_2 - u_1} \right) \quad . \quad (4.2)$$

In the experiments in which a copper tamper is used, an extra step is required to infer the reshock state from the measured state, which lies at lower pressure along the copper release path. The reshock state parameters are tabulated with the initial shock states in Table 4.1. Uncertainties in the first shock state were propagated with the additional experimental uncertainty associated the particle velocity measurement.

The most complete set of data is on the RS234 mixture. These data are plotted together in the P-u plane in Figure 4.11. The first and second shock states are plotted as closed circles and open squares, respectively. The uncertainties are smaller than the symbol size for the first shock states. The actual particle velocities taken from each VISAR measurement are plotted on the LiF Hugoniot for experiments TWP-2, TWP-4, and TWP-7, and on the zero-pressure axis for TWP-

10 and TWP-11, the two experiments which made use of free-surface measurements. From this plot it can be seen graphically how the second shock states were determined.

Table 4.1: Shock and Reshock State Parameters for RS234 Experiments

Exp #	State	U_s (km/s)	+/-	u_p (km/s)	+/-	P (GPa)	+/-	ρ (g/cm ³)	+/-	V/V ₀	+/-
TWP-2	First	4.230	0.220	1.937	0.021	14.15	0.36	3.187	0.178	0.985	0.055
TWP-2	Second	6.653	0.615	1.390	0.020	25.76	0.47	3.472	0.196	0.904	0.051
TWP-4	First	4.020	0.180	1.943	0.021	13.49	0.35	3.343	0.181	0.939	0.051
TWP-4	Second	6.151	0.379	0.806	0.006	36.88	0.40	4.102	0.229	0.766	0.043
TWP-7	First	2.690	0.080	1.204	0.023	5.60	0.20	3.127	0.131	1.004	0.042
TWP-7	Second	5.302	0.321	0.445	0.007	18.19	0.33	3.650	0.158	0.860	0.037
TWP-10	First	2.690	0.080	1.221	0.023	5.67	0.20	3.162	0.134	0.993	0.042
TWP-10	Second	5.160	0.384	0.447	0.013	18.29	0.61	3.719	0.166	0.844	0.038
TWP-11	First	3.940	0.170	1.883	0.020	12.81	0.34	3.308	0.171	0.949	0.049
TWP-11	Second	6.935	0.655	0.814	0.030	37.33	1.72	3.910	0.214	0.803	0.044

In addition to the purely experimental data, a calculated Hugoniot was plotted for the powder. This calculation was based on a simple snowplow model, which assumes that the material has no strength, and that the first shock completely crushes the powder to the theoretical maximum density of its components. This Hugoniot assumes that no reaction has taken place. The first shock states for the two lower-pressure experiments are indistinguishable from the inert snowplow Hugoniot. The first shock states for the three higher pressure experiments all lie beneath the same calculated curve, implying that they all reached a higher density than the theoretical maximum zero-pressure density. This is fully consistent with the expected behavior of a low-strength, inert, compressible mixture.

These shock and reshock states have also been transformed to the P-V plane, and plotted in Fig. 4.11. In this figure, the vertical line denotes the zero-pressure specific volume at TMD. Each shock state is linked to its reshock state by a dotted line. It can immediately be seen from the data in this plane that a purely mechanical model is inadequate to describe this material. If there were no thermal pressure component, then all points would lie on a single curve. By contrast, there is a large thermal offset. This is most readily seen by comparing the initial shock states of the three higher pressure experiments to the Rayleigh lines connecting the shock and reshock states of the other two shots. At a given density, the three shock states lie well above the Rayleigh lines; the pressure difference is due to the thermal contribution from the much higher internal energy associated with the much-higher-pressure initial shock into the porous material. These issues have been discussed at length (Boslough 1990, 1991) for shock compression of porous powder mixtures.

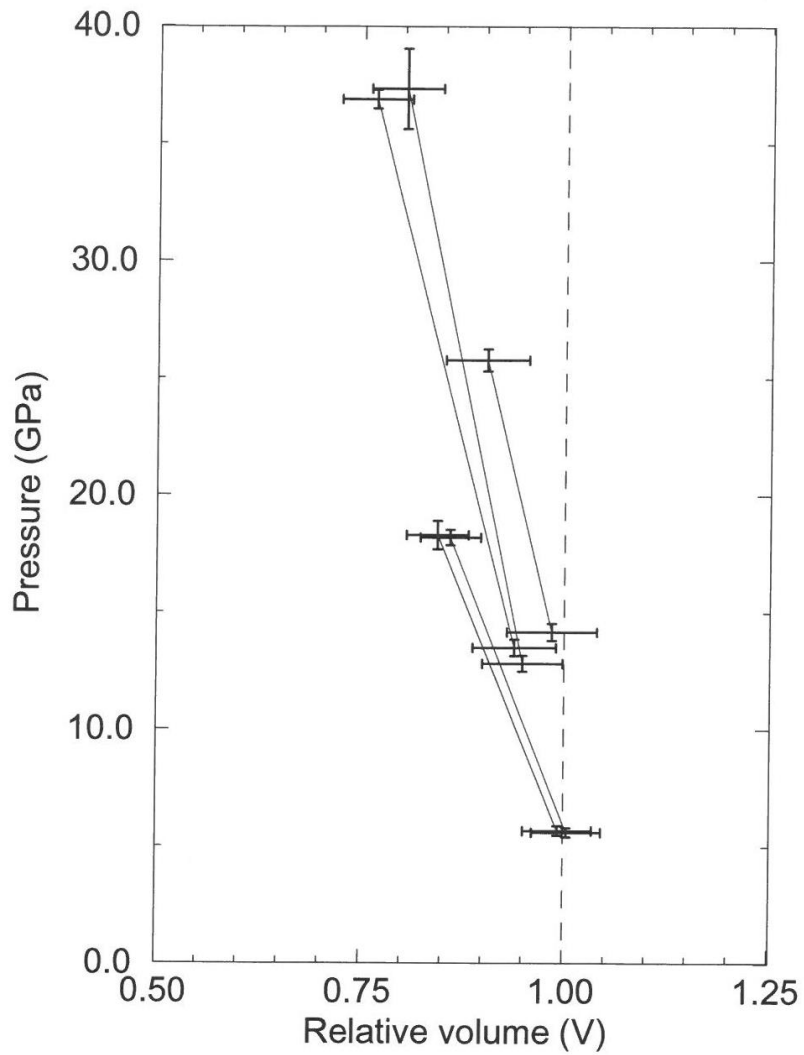


Figure 4.11 – Shock and reshock states of five RS234 experiments transformed to P- V plane. The vertical dashed line denotes the fully crushed volume of the reactants at zero pressure.

5. EARLIER EXPERIMENTAL WORK

Much of the impetus for doing the present work came from the results of R.A. Graham and coworkers (unpublished, 1993), who reported strong reactions in similar powder mixtures under similar experimental conditions but at lower shock pressures. The evidence for the reported reactions was taken from PVDF-gauge data recorded during transit of a first shock through powder compacts, before any release. Because other experiments, including those presented in the present report, have failed to produce evidence for strong shock-induced reactions under similar conditions, we have reexamined a subset of the data on which the conclusions of strong reactivity were based. For the reasons discussed below, our interpretation of the data we examined is different. We conclude that these earlier experimental results do not provide evidence for strong shock-induced chemical reactions.

In Figure 5.1, the experimental configuration of some of the earlier experiments is schematically illustrated, as one variation described by Anderson et al. (1994), Holman et al. (1994), and Dunbar et al. (1994). We have analyzed a subset of four experiments, all of which made use of this configuration. A 6.35-mm copper flyer plate impacted the target, which consisted of a 6.35-mm driver, followed by a powder sample about 3.8 mm thick, which was backed by a copper tamper 9.52 mm thick. Two PVDF gauges were used to measure the stress: an input gauge at the driver/powder interface, and an output gauge at the powder/tamper interface. The input gauge was protected from the powder by a layer of PTFE (Teflon) about 0.1 mm thick. The inset in Figure 5.1 shows the details of shock interactions shortly after the first arrival at the input gauge. Because the porous powder is initially at lower density (and shock impedance) than the PTFE/PVDF gauge package, the first shock reflects from the PTFE/powder interface and returns to the gauge as a rarefaction wave. The gauge package experiences multiple rarefactions until it achieves mechanical equilibrium with the shocked and partially-released sample.

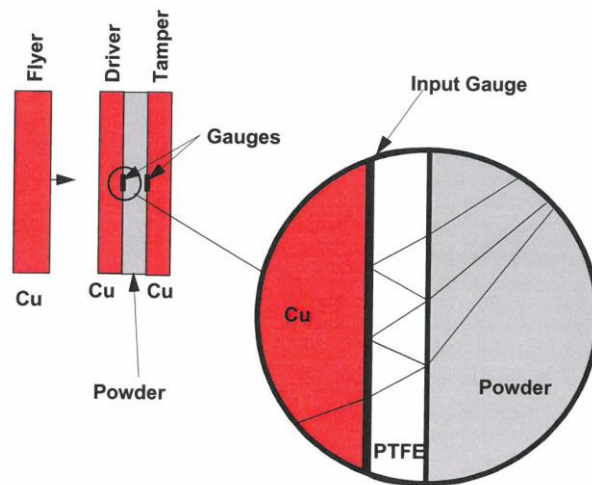


Figure 5.1 – Schematic representation of experimental configuration of PVDF experiments.

A more detailed description of the wave interactions is shown in Figure 5.2. The distance-time plot on the left shows the sequence of states experienced by the powder and measured at the gauge. State (2) is the initial state seen at the gauge, as determined by the intersection of copper centered at the impact velocity and initially stationary PTFE (neglecting the small difference between PVDF and PTFE Hugoniot). State (3) is the first shock state in the powder, which releases down the much steeper curve dictated by the properties of compacted powder. This is illustrated schematically in the stress/particle-velocity plot on the right-hand side of Figure 5.2. The gauge package rings down to "final" state (F). However, because the rarefaction waves in the compacted powder move at a higher velocity than the initial shock wave, they eventually overtake it and decay it to the level dictated by "end" state (E), the state it would have achieved had the gauge package not been present. *This* is the state that the gauge eventually settles on when full mechanical equilibrium is achieved after several full reverberations.

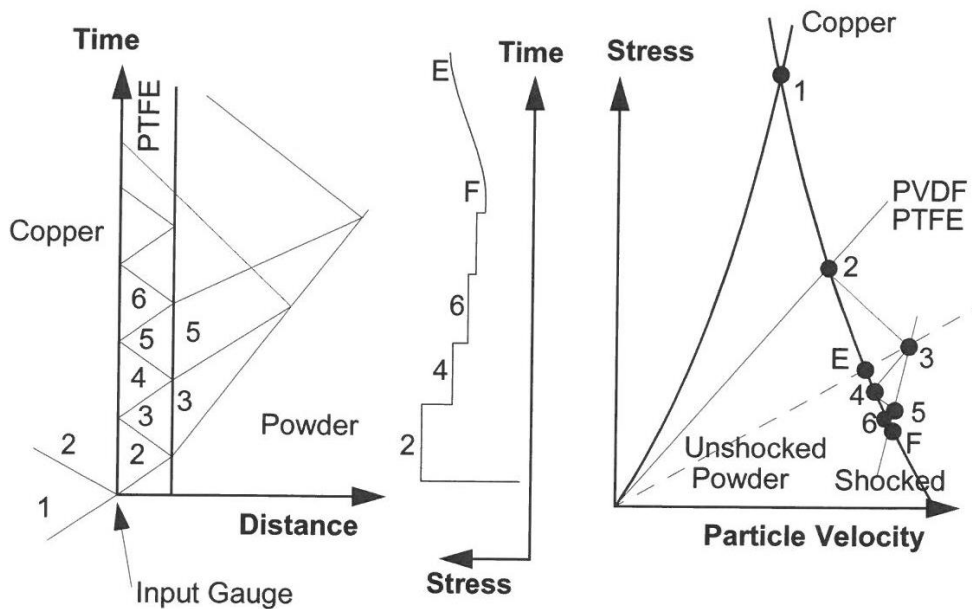


Figure 5.2 – Schematic loading history in PVDF experiments, showing distance-time diagram, stress history, and stress/particle velocity-diagram.

We analyzed the input PVDF records from four experiments, and the resulting stress histories at the gauges . The stress histories demonstrate overall behavior that is qualitatively consistent with that expected on the basis of Fig. 5.2. In all but one case, the state that would be identified as state (E) lies at higher pressure than that identified as state (4). In all four cases, the pressure used in the previous analysis to determine P-V states was the state we have identified as (4) in Figure 5.2, which is not in mechanical equilibrium with the sample.

The jump conditions which express conservation of mass and momentum across a steady shock front can be written:

$$\rho_{oo}U = \rho(U-u) \quad (\text{conservation of mass}) \quad (5.1)$$

$$P = \rho_{oo}Uu \quad (\text{conservation of momentum}) \quad (5.2)$$

where ρ_{oo} is the initial density, ρ is the final density, P is the shock pressure, and u and U are particle and shock velocity, respectively .

Combining these two equations yields an expression for the specific volume (V) behind the shock front, if P and U are independently determined:

$$V/V_o = (1-(P/\rho_{oo}U^2)) \times (V_{oo}/V_o) \quad (5.3)$$

where $V_{oo}= 1/\rho_{oo}$ is the specific volume of the distended (porous) initial state, and $V_o= 1/\rho_o$ is the specific volume of the fully densified mixture of the same composition.

In the earlier analysis, in addition to pressure determined as described above, shock velocities were extracted from the known times of arrival at the input and output gauges, and the initial thickness of the sample. By inserting these independently-determined P and U values into equation 5.3, the P-V states were determined. However, there are several problems with this method. First, as pointed out above, the pressure chosen from the input gauge data is not in mechanical equilibrium with the shocked powder and is not representative of it. Second, equation 5.3 comes directly from the jump conditions, which are valid only for a steady shock; this is not necessarily the case here. Third, the determination of shock velocity from transit time assumes that the shock velocity is constant, which is only true for a steady wave. In fact, because of the effect of the gauge package on the input shock, we know a priori that the wave is not steady.

Fortunately there is more information for each experiment that was not used to help determine the P-V states. By checking for self-consistency, this additional information can be used to determine whether the unsteady wave generated by gauge-package reverberation is a small transient perturbation or whether it dominates the wave propagation. Since the impact velocities and shock impedances of the impactor/driver materials are known in all cases, the equilibrium particle velocity for the sample can be extracted by impedance matching. Combining this with equation 5.2 reduces determining the P-V state to the measurement of one independent variable, either P or U . If both are measured, they

must agree; if they do not agree then at least one of the assumptions has been violated. That would mean that one or both of the following must be true. 1) The unsteady behavior dominates the wave propagation and the jump conditions do not even approximately apply. 2) The transformation of PVDF data to pressure is in error.

These are the issues that were brought up during the review process of a series of papers in which similar experimental data were published (Anderson et al. 1994, Holman et al. 1994, Dunbar et al. 1994). The need was communicated to the principal authors to apply conventional analysis to the data, and to explain in the papers why such an analysis should be rejected. According to Anderson et al. (1994), momentum is not conserved in the experiments due to wave dispersion, and the jump conditions therefore do not apply. Nevertheless, it is asserted without reference or rigorous argument in that paper that the relative volume can be determined from the measured shock velocity and stress. This is done in the paper, presumably by using equation 5.3. However, this equation is derived directly from the conservation-of-momentum jump condition, equation 5.2, which was said to not apply.

Moreover, in the papers by Holman et al. (1994) and Dunbar et al. (1994), certain values are stated to have been calculated using a Hugoniot program (or based on predictions) rather than actual measurements. Unfortunately, only one of these values is tabulated and plotted, with no explanation as to why this method of analysis was appropriate for this particular experiment and not for the others. The lack of presentation of stress histories from these experiments prevents an independent determination of these values, and it is therefore impossible to evaluate the treatment of the data or the conclusions of the papers. We strongly recommend that if these data are ever published, either as a full report or in a peer-reviewed journal, that full stress-history data be included so that the conclusions can be independently evaluated.

In Figure 5.3, the P-V states for four experiments, as determined by the earlier analysis, are plotted as triangles. These points, combined with similarly-determined points from the rest of the data set, were used to define and determine a locus of states called the "ballotechnic curve" by Graham et al. (1993). On the same graph are P-V states as determined by two other methods. The open circles were calculated from the measured pressures of Graham et al. (unpublished data, 1993), and the closed circles from the shock velocities from the same source inferred from times of arrival. In both cases the impact velocity was used to determine particle velocity. It should be noted that these independently determined values for P and U are both in error for reasons addressed above, but the error in U associated with the transient decay of the shock is probably much smaller.

As can be seen in Figure 5.3, the re-determined P-V states all lie to the right of the zero- pressure TMD of the powder mixture, as would be expected for partial compaction. The states determined from the shock velocities have less scatter, and they show a general trend of density increasing with shock pressure, as would be expected. This reanalysis also removes the unexplained anomalously high densities of the two lowest-pressure experiments.

Improved P-V states can be still be extracted from this data set by determining the time it takes for mechanical equilibrium to be reached from the recorded stress histories, and using them to make corrections to the shock velocity. Shock pressures associated with this state can be independently taken from the same stress histories, assuming the PVDF measurements are accurate, and will provide confirmation.

Only a small subset of all the data obtained by this type of experiment for these materials has been revisited. Since similar high-quality experimental data sets exist, it would be useful to recalculate P-

V states for every such test.

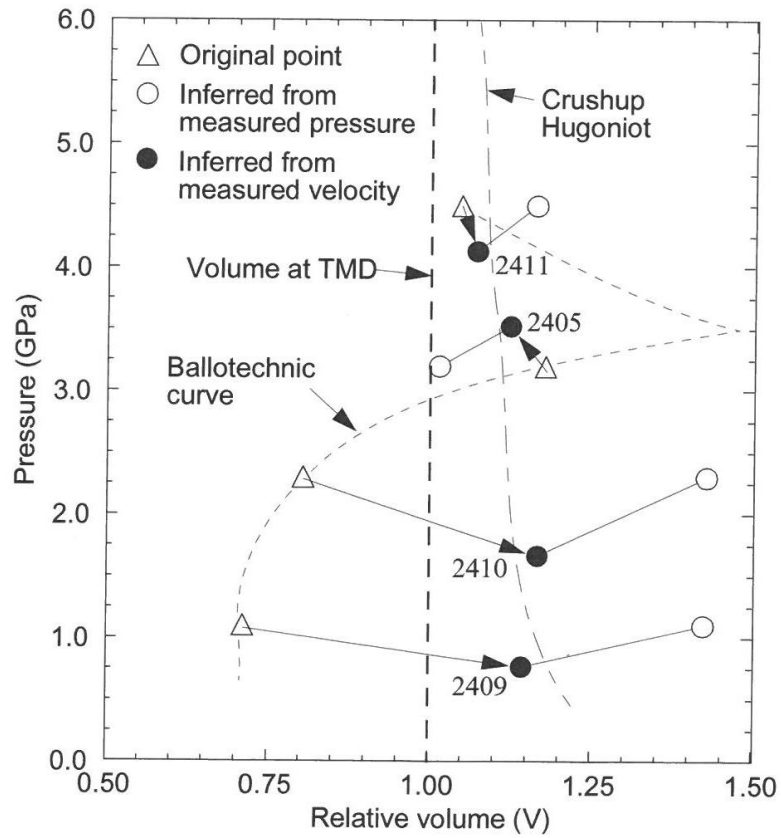


Figure 5.3 – Data from unpublished PVDF experiments on 50% TMD reactive powders and ballotechnic curve defined by Graham et al. (1993) with P-V states recalculated from original data.

6. CONCLUSIONS

The results of the experiments presented in this paper do not provide evidence that shock-induced chemical reactions have taken place for the duration of the shock loading under any of the conditions tested. Control experiments on single-component inert materials show time-dependent behavior that is similar in character and magnitude to that observed in the same experiments on the reactive formulations. Comparison of experimental data to output of numerical simulations using inert and reactive models is of limited use for highly porous powder mixtures unless the large thermal components are taken into account. The difference between the predicted and measured particle-velocity histories can, in all cases, be attributed to causes other than chemical reactions between components. Free surface "ring-down" experimental configurations are likely to be the most sensitive to highly expandable reaction products, but control experiments on inert substitutes must be performed to distinguish such products from heterogeneous vaporization or contribution from pore gases or volatile contaminants.

A review of previous experimental data has also failed to produce sufficient evidence for prompt shock-induced chemical reactions in the tested materials. Unpublished pressure-volume states that have been used as evidence for shock-induced chemical reactions are sufficiently in error to call this conclusion into question, and published P-V states are based on inappropriate data reduction methods. The subset of these data which were re-analyzed by conventional impedance-matching methods are consistent with a compressed but unreacted mixture.

It is important to make a strong distinction between a lack of evidence, as we present in the present paper, and a proof of no reaction. We have not demonstrated that reactions are not taking place, but we believe that all the data discussed here are consistent with well-established phenomena that do not involve reactions. In this sense, the conclusions of this report are indefinite; we have neither demonstrated that reactions take place, nor that they do not, for the duration of the shock loading. However, application of Occam's razor requires the burden of proof to rest on an unambiguous demonstration that they do take place. Acceptance of such an interpretation should require the full disclosure of the experimental data on which it is based, along with performance of requisite control experiments.

7. RECOMMENDATIONS

Any further work in this area should: 1) attempt to answer some remaining questions to either strengthen the above conclusions, or to find possible weaknesses in them, 2) attempt a proof-of-principle experiment that will conclusively demonstrate an example of the shock-induced chemical reactions that have been postulated .

It may be possible to accomplish the first goal with a single experiment. It would essentially be a control experiment on one of the components of RS234. Our current hypothesis is that vapor produced either by decomposition, impurities, or trapped air (or a combination thereof) is sufficient to explain the data without requiring a reaction between components. A positive result on one control experiment would be sufficient to answer this question.

The second goal would require a short series on a very fine-particle mixture that would be likely to have much faster reaction kinetics. There is experimental evidence that certain mixtures of very-fine particles can indeed react on timescales of interest. This is certainly true in the limit of particle size going to zero. In this sense, the question is not whether such reactions take place, but whether the threshold particle size is large enough to be useful. One possible experiment would be to repeat the five-shot series on a finer-particle version of RS-234, to give a direct basis for comparison. A dramatic difference in Hugoniot states and release paths would provide strong evidence for the postulated rapid reactions. It is very important to establish, unambiguously, the existence of such reactions, and to provide the raw experimental data for independent evaluation by others.

REFERENCES

1. Anderson, M.U., Graham, R.A., and Holman, G.T., "Time-Resolved Shock Compression of Porous Rutile: Wave Dispersion in Porous Solids," in *Shock Compression of Condensed Matter--1993*, edited by S.C. Schmitt et al. (AIP Press, New York, 1994) pp 1111-1114.
2. Barker, L.M. and R.E. Hollenbach, "Shock-Wave Studies of PMMA, Fused Silica, and Sapphire." *J. Appl. Phys.*, 41, 4208 (1970).
3. Batsanov, S. S., Doronin, G. S., Klochkov, S. V., and Teut, A. I., "Synthesis Reactions Behind Shock Fronts." *Combustion, Explosion, and Shock Waves*, 22, 765 (1986).
4. Boslough, M. B. and Graham, R. A., "Submicrosecond Shock-Induced Chemical Reactions in Solids: First Real-Time Observations ." *Chem. Phys. Lett.*, 121, 446 (1985)
5. Boslough, M. B. "A Thermochemical Model for Shock-Induced Chemical Reactions (Heat Detonations) in Solids." *J. Chem. Phys.* 92, 1839 (1990)
6. Boslough, M. B., "A Thermochemical Model for Shock-Induced Chemical Reactions in Porous Solids: Analogs and Contrasts to Detonations," in *Proceedings Ninth Symposium (International) on Detonation*, (Office of the Chief of Naval Research, 1991) pp 1199-1216.
7. Boslough, M. B. "Thermochemistry of Shock-Induced Exothermic Reactions in Selected Porous Mixtures." in *Proceedings of Explomet '90 International Conference on Shock-Wave and High-Strain-Rate Phenomena in Materials*, edited by M. A. Meyers et al. (Marcel Dekker, New York, 1992a), pp. 253-260.
8. Boslough, M. B. "Postshock Spectral Radiance Measurements in Nickel and Nickel/Aluminum Powders." in *Shock Compression of Condensed Matter--1991*, edited by S. C. Schmitt et al. (North-Holland, Amsterdam, 1992b) pp. 617-620.
9. Crawford, D.A., unpublished (1993)
10. Dunbar, E., Graham, R.A., Holman, G.T., Anderson, M.U., and Thadhani, N.N. "Time-Resolved Pressure Measurements in Chemically Reacting Powder Mixtures." in *Shock Compression of Condensed Matter--1993*, edited by S.C. Schmitt et al. (AIP Press, New York, 1994) pp 1303-1306.
11. Graham, R. A., Morosin, B., Venturini, E. L., and Carr, M. J., "Materials Modification and Synthesis under High Pressure Shock Compression." *Annu. Rev. Mater. Sci.* 16, 315 (1986).
12. Graham, R. A. "Ballotechnic Materials." Sandia National Laboratories, SAND88-1055 ; Albuquerque, New Mexico; 1988.
13. Graham, R. A., Anderson, M. U., Horie, Y., You, S-K., and Holman, G. T., "Pressure Measurements in Chemically Reacting Powder Mixtures with the Bauer Piezoelectric Polymer Gauge." *Shock Waves*, 3, 79 (1993)

14. Holman, G.T., Graham, R.A., and Anderson, M.U., "Shock Response of Porous 2Al + Fe₂O₃ Powder Mixtures." in Shock Compression of Condensed Matter--1993, edited by S.C. Schmitt et al. (AIP Press, New York, 1994) pp 1119-1122
15. Horie, Y. "Shock-Induced Solid State Chemistry: Theoretical Background." Sandia National Laboratories, SAND86-0922; Albuquerque, New Mexico; 1986.
16. Horie, Y. and Kipp, M. E. "Modeling of Shock-Induced Chemical Reactions in Powder Mixtures." J. Appl. Phys., 63, 5718 (1988).
17. Hornig H., Kury J., Simpson, R., Helm, F., and von Holle, W. "Shock Ignitions of Pyrotechnic Heat Powders." in Proceedings of the Eleventh International Pyrotechnics Seminar, (1986), p. 699.
18. Marsh, S.P., LASL Shock Hugoniot Data, U. California Press (1980), 658 pp.
19. Schmalzried, H., Solid State Reactions, Verlag Chemie (1981), 254 pp.
20. Rice, M. H., McQueen, R. G., and Walsh, J. M., "Compressibility of Solids by Strong Shock Waves." Solid State Physics, 6, 1 (1958).
21. Sheffield, S. A., and Schwarz, A. C. in Proceedings of the Eighth International Pyrotechnics Symposium, edited by A. J. Tulis (IIT Research Institute, Chicago, 1982), p. 972.
22. Young, R. and Silling, R., "Experimental Technique to Obtain Material Response at Strain Rates to 10⁵s⁻¹." in Shock Compression of Condensed Matter--1993, edited by S.C. Schmitt et al.(AIP Press, New York, 1994) pp 1647-1650.
23. Yoshida , M., "Microscopic Observations of Shock Compression in Powders." in Proceedings of the NIRIM International Symposium on Advanced Materials '94, edited by M. Kamo et al. (International Communications Specialists, Tokyo, 1994) pp. 85-88.
23. Vandermolen, W.B., Mulligan, E.J., and Patton, R.J., SNL memo to S.H. Fischer, (1993) (CNSI).

DISTRIBUTION

1	MS0899	Technical Library	9536 (electronic copy)
---	--------	-------------------	------------------------



Sandia National Laboratories